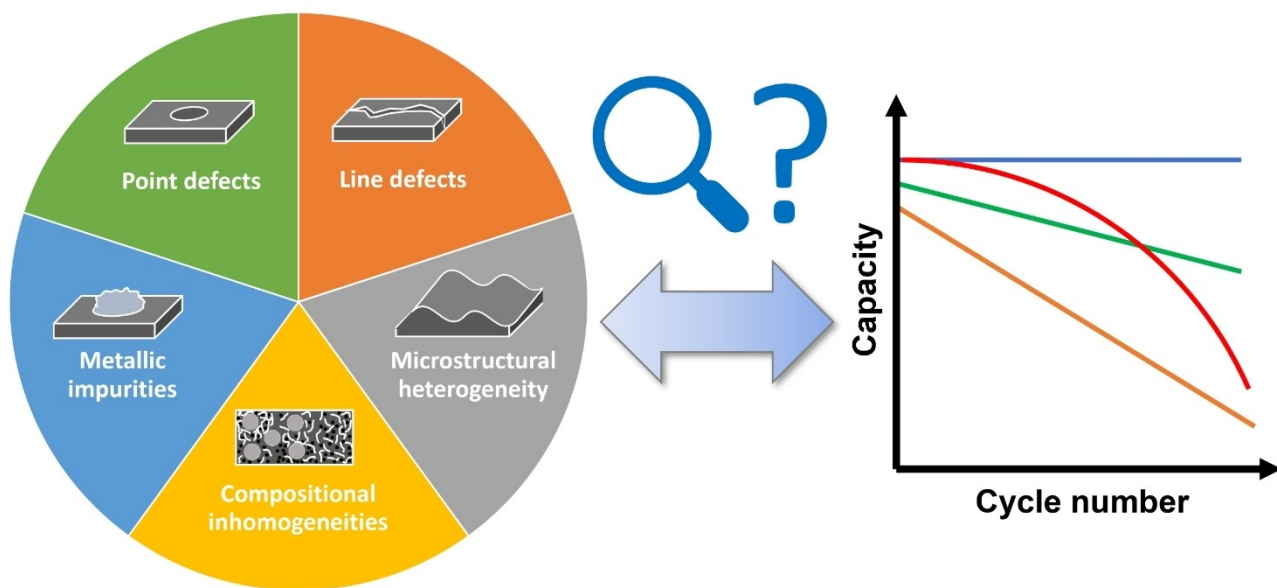


# Impact of Electrode Defects on Battery Cell Performance: A Review

Arnaud du Baret de Limé,<sup>[a]</sup> Tobias Lein,<sup>[b]</sup> Sebastian Maletti,<sup>[b]</sup> Karoline Schmal,<sup>[b]</sup> Sebastian Reuber,<sup>[a]</sup> Christian Heubner,<sup>[a]</sup> and Alexander Michaelis<sup>[a, b]</sup>



The continuing rise of electric mobility is driving demand for lithium-ion batteries to unprecedented levels. To ensure efficient production of high quality, yet affordable battery cells, while making the best use of available raw materials and processes, reasonable quality assurance criteria are needed. A step of particular importance, affecting all downstream processes, lies in electrode manufacturing including mixing, coating, drying, and calendering. Several classes of defects which originate in these processes are well-known and detectable using various methods. The crucial point, however, lies in the

quantification of their electrochemical significance, i.e., in an evaluation, which defect types, sizes and concentrations can be tolerated without impacting cell performance. Herein, we review the still scarce literature on that topic. It is found that, although the impact of some defects is quite well understood, others almost completely lack an evaluation of their criticality. We finally make suggestions for further studies paving the way to deduce knowledge-based quality assurance criteria for the large variety of coating defects occurring in lithium-ion battery electrodes.

## 1. Introduction

Li-ion batteries (LIBs) have become the energy supply backbone of today's portable electronic devices, electric vehicles and stationery (micro-)grid storage.<sup>[1,2]</sup> The current trend of decarbonization in the mobility sector will lead to a tremendous demand and increase in Li-ion battery production.<sup>[3]</sup> Following recent predictions, electric vehicles alone will require ~6 TWh of battery capacity annually by the year 2050,<sup>[4]</sup> corresponding to roughly 170 times the theoretical output of Tesla's Nevada Gigafactory. Considering production rates of this magnitude, any few percent scrap rate would correspond to a loss of several billions of dollars, assuming the current average cell cost of 140 \$ kWh<sup>-1</sup>.<sup>[1]</sup> Apart from monetary savings, thousands of tons of scarce resources will be preserved and the mining impact on the environment can be kept at a minimum, when scrap rates are reduced.

Currently, scrap rates in battery production are reported to range between 5% and 30% or even more, depending on the manufacturer.<sup>[5,6]</sup> Especially during the ramp-up of production and introduction of innovative processes and machinery, the scrap-rate can be very high. Lowering scrap-rate, along with other optimization strategies, will be required to reach strategic targets, such as a battery price of less than 80 \$ kWh<sup>-1</sup>.<sup>[7]</sup> Scrap originates from various reasons and different steps in battery manufacturing, such as unsatisfactory raw material quality, the electrode production process, the stacking or winding of cells or even further downstream processes, such as packing or formation.<sup>[6]</sup> As a step of particular importance, the present review focuses on the electrode production, including mixing, coating, drying and calendering. During recent years, numerous detection methods have become available, allowing to trace defects of different types and sizes either in-line, i.e., directly

during production, or off-line.<sup>[8–11]</sup> In many cases, however, it is not clear how a particular defect will actually affect the electrochemical performance of the electrode or cell.

Figure 1 shows a sorting concept of intermediate products during electrode manufacturing depending on the criticality of specific defects. Intermediate products exhibiting non-critical defects or deviations from the norm may be further processed and later commercialized as second-grade good rather than scraped. Critical defects (e.g., responsible for severe performance or safety issues) must however be rooted out as soon as possible. Therefore, comprehensive knowledge about the impact of defect type, size, and quantity on the electrode and cell performance is a crucial for developing efficient quality assurance systems and to improve process control. In this review, we compile the sparse literature on this topic, highlighting the importance and need to further explore the relationships between coating defects and the electrochemical behavior of electrodes. Understanding these relationships is urgently needed for developing effective inline quality assurance to safely reject defective electrodes that affect cell lifetime or safety, or to effectively make process adjustments to reduce scrap rates.

## 2. Battery Electrode Manufacturing and Quality Assurance

### 2.1. Electrode manufacturing

Large lithium-ion batteries, for example in the context of electromobility applications, typically consist of one or more battery packs that contain multiple battery cells. Such automotive cells currently have a variety of different geometries and require their power to be precisely regulated (load distribution, thermal evolution).<sup>[13]</sup> The most expensive parts of the battery cells are the anode and cathode, which together account for 64% of the cell's material costs, while the rest is accounted for by separator, electrolyte and housing parts.<sup>[12]</sup> The high cost of electrodes stems from the high price of active materials (~72%) as well as from the manufacturing process (~26%). Among the manufacturing costs for battery cells, electrode production, which is the focus of this work, accounts for approximately 39% and is thus above the costs for cell

[a] A. du Baret de Limé, Dr. S. Reuber, Dr. C. Heubner, Prof. A. Michaelis  
Fraunhofer Institute for Ceramic Technologies and Systems IKTS  
Winterbergstr. 28, 01277 Dresden, Germany  
E-mail: arnaud.du.baret.de.lime@ikts.fraunhofer.de

[b] T. Lein, Dr. S. Maletti, K. Schmal, Prof. A. Michaelis  
Institute for Materials Science  
TU Dresden  
Helmholtzstr. 7, 01062 Dresden, Germany

© 2022 The Authors. *Batteries & Supercaps* published by Wiley-VCH GmbH.  
This is an open access article under the terms of the Creative Commons Attribution License, which permits use, distribution and reproduction in any medium, provided the original work is properly cited.

assembly (28%) or formation/aging (33%).<sup>[14]</sup> In a first step, the active materials [e.g., graphite,  $\text{LiNi}_x\text{Mn}_{1-x}\text{Co}_2\text{O}_2$  (NMC xyz),  $\text{LiFePO}_4$  (LFP)] are mixed with a conductive additive (e.g., carbon black), a polymeric binder (e.g., polyvinylidene difluoride (PVDF), cellulose or latex based components) as well as the corresponding aqueous or organic solvent (e.g., N-Methyl-2-pyrrolidone (NMP)) into a homogeneous electrode slurry. To achieve the desired homogeneity, the use of mixing tools and corresponding process sequences is necessary. Inadequate mixing forces and times may result in inhomogeneous distribution of the material, leading to undesirable agglomerates. Conversely, excessive mixing can result in damage to the most sensitive components, typically the polymer chains of the binder or the surface of the particles. In addition, the resulting viscosity of the slurry must be suitable for the subsequent coating step. Compound-related defects, such as agglomerates resulting from improper particle or carbon black dispersion, are

irreversible and cannot be compensated for in subsequent processes. Therefore, a detection mechanism before coating is necessary to allow options such as scraping the slurry or reprocessing it. The electrode slurry is cast as a thin layer (100–500  $\mu\text{m}$ ) onto a metallic substrate (current collector) using a slot-die or a doctor blade.<sup>[15]</sup>

Figure 2(a–c) illustrates several typical defects that may appear in the coating stage: Agglomerates and impurities of sufficient size in the slurry may lead to a localized obstruction of the slot-die, forming streaks in the electrode layer. Air entrapment while mixing or casting can result in the formation of elliptical defects of different sizes due to bubbles. A faulty parametrization of the slot-die (gap to thickness ratio, slurry flowrate or pressure) may lead to an undesired pattern in the electrode layer (chatter, ribbing). Electrode misalignment due to unprecise coating on the collector foil is also a cause for rejecting the resulting cells that may otherwise present a



Arnaud du Baret de Limé received his Engineering Diploma from the École Centrale de Lille in France and his Master of Science degree (Materials Science) from the Technical University of Berlin in 2016. He has been working as a research associate at the Fraunhofer IKTS in Dresden in the domain of electrode development since 2018. His current area of research is the detection and prevention of defects in battery manufacturing.



Tobias Lein received his Master of Science degree (Chemistry and Energy) in 2018 from the University of Applied Science Zittau/Görlitz under the supervision of Professor Klaus Seibt and Professor Jens Weber. He is now a PhD candidate under the guidance of Professor Alexander Michaelis at TU Dresden in collaboration with Fraunhofer IKTS. His current research interests focus on Li-ion and Na-ion batteries.



Sebastian Maletti received a diploma degree in Materials Science at TU Dresden (Germany) in 2017 and worked at the Leibniz Institute for Solid State and Materials Research, graduating with a PhD thesis about post-Li battery concepts. In 2020, he started as a postdoctoral fellow at the chair of Inorganic Nonmetallic Materials at TU Dresden, belonging to the working group combinatorial microelectrochemistry. Sebastian's research interests focus on development of energy storage materials and advanced electrochemical characterization methods.



Karoline Schmal received her diploma in chemical engineering at the Technical University of Dresden in 2022 under the supervision of Professor Alexander Michaelis with the focus on inhomogeneities in electrodes for lithium-ion-batteries. She previously worked in validation at Arevipharma in Dresden, and quality assurance at Covestro in Antwerp, Belgium. She will now start her career in the renewable energy sector.



Sebastian Reuber studied process engineering at University of Applied Sciences Gießen (Germany) and TU Dresden and received his doctorate in 2013 on design optimization of high-temperature solid oxide fuel cells. He was co-founder and CTO of a start-up company developing mobile fuel cell systems for off-grid power supply until 2017. Then he joined the department Mobile Energy Storage Systems and Electrochemistry of the Fraunhofer IKTS managing the Electrode and Process Development Group. Sebastian has more than 15 years of experience in the field of fuel cells, Li-ion batteries, and supercapacitors.



Christian Heubner graduated from TU Dresden as a chemical engineer in 2012 and received his Ph.D. in materials science 2016 under supervision of Professor Alexander Michaelis. He worked as a postdoctoral fellow at the Institute of Materials Science (TU Dresden) and joined the department Mobile Energy Storage Systems and Electrochemistry of the Fraunhofer IKTS in 2019. His research interests mainly focus on electrochemistry and modelling of materials for energy storage, including Li-ion and next generation batteries.



Alexander Michaelis received his degree in physics and PhD in electrochemistry from the University of Düsseldorf (Germany). Since 2004, he is president of the Fraunhofer Institute for Ceramic Technologies and Systems IKTS and holds the chair of Inorganic Nonmetallic Materials at Technische Universität Dresden. In 2015 he was appointed for the LEE HSUN Award on Materials Science. He is Fellow of the American and the European Ceramic Society. In 2019 he was elected President of the German Ceramic Society. He holds more than 40 patent families in materials science, microelectronics and electronics, and provided more than 360 publications.

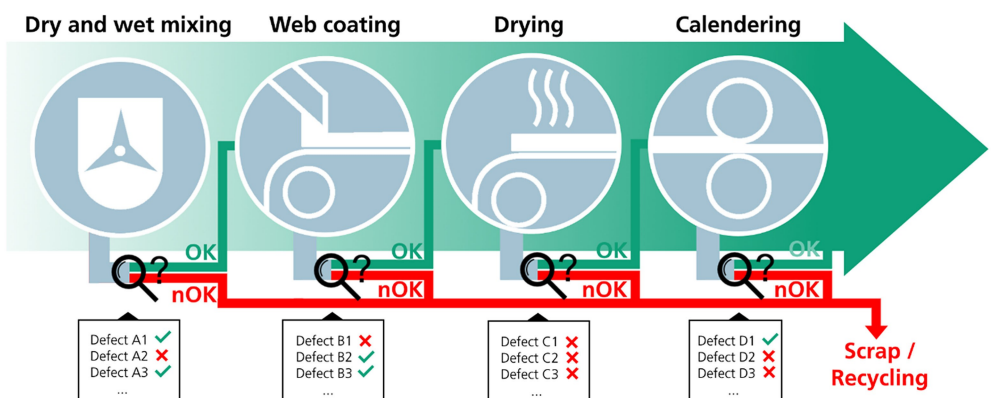


**Figure 1.** Sorting concept of intermediate products in the electrode manufacturing depending on the criticality of specific defects. Intermediate products containing defects that are however not critical to the application may be further processed and later commercialized as second-grade good rather than scrapped. Critical defects (e.g., responsible for severe performance or safety issues) must however be rooted out as soon as possible. Adapted from Ref. [12] with permission. Copyright (2018) Springer Nature.

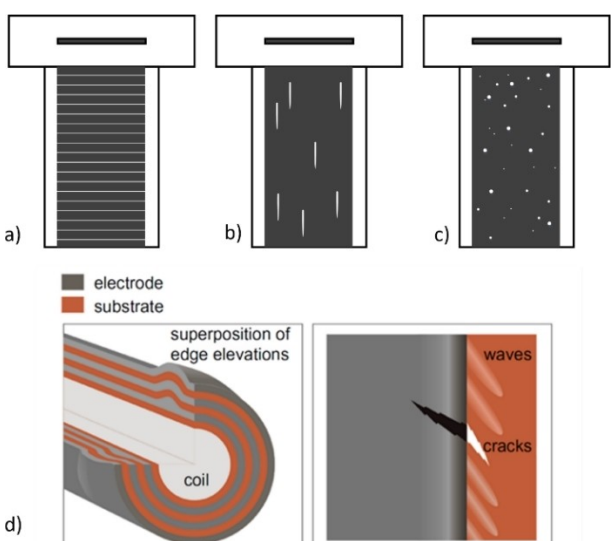


**Figure 2.** Examples of coating-related defects in electrode processing:  
a) chatter, b) streaks, c) bubbles and d) the effect of edge defects on winding and calendering. Adapted from Ref. [16] with permission. Copyright (2021) The Authors, published by Springer Nature.

security risk.<sup>[7]</sup> High precision is required to reach the desired electrode loading while ensuring a uniform coating geometry. Elevated coating edges for example detrimentally affect downstream processes such as coil winding or calendering, leading to cracks in the electrode layer as well as deformation or tearing of the current collector (Figure 2d).<sup>[16]</sup>

The coating step is followed by the drying of the electrode layer, typically using convective methods such as heated laminar air flows. This step, additionally to being a production bottleneck, is the most energy intensive step since significant quantities of solvents must be removed from the electrode while the structure is being formed.<sup>[14]</sup> Here, the temperature profile and web speed are essential parameters which determine the repartition of the binder throughout the electrode. Improper drying can result in binder migration and reduced adhesion to the collector foil, which negatively affect

the specific capacity and cycle life of the battery.<sup>[17]</sup> Thick electrodes for high energy cells are especially susceptible to cracking during the drying process.<sup>[18]</sup>

After drying, the electrode layer is compacted by two high precisely machined rolls in a roll-to-roll calendering process. This step is necessary to reduce the porosity of the electrode layer and improve the resulting energy density. It requires a high line load due to the toughness of the material, especially in high-energy electrodes designs where porosity  $\leq 10\%$  may need to be achieved.<sup>[19]</sup> Defects at this stage are usually a variation of the electrode foil deforming or tearing, due to pre-existing imperfections in the substrate and electrode layer in combination with high mechanical stress during calendering.<sup>[20]</sup> Furthermore, local disparities in electrode porosity may appear in case of inhomogeneous mass loading during coating. Microstructural changes, such as particle cracking or the closing of surface pores, may also occur. These defects are difficult to detect inline and may therefore fall under the radar during manufacturing. Beside the type and size of the defect, the frequency of occurrence must also be taken into account during process ramp up. Regarding the active influencing of the occurrence and frequency of defects, process-related measures, in addition to the selection of materials, are the most important. For example, the mixing time or intensity can be increased at the expense of increased energy and time consumption to reduce the occurrence of agglomerates and any resulting line defects. Comparably, inhomogeneities of the microstructure and mass loading can be regulated by the speed of the coating, drying and calendering processes.

## 2.2. Quality assurance

Quality assurance is of utmost importance in battery production due to the high number of consecutive steps in the process chain. Furthermore, the manufacturing process from raw materials to complete battery packs takes up to two weeks, resulting in significant and costly interruption of production if a defect is detected late in the process chain.<sup>[13]</sup> To address this

issue, efforts in the academic world have focused in last years on establishing quality gates concepts that circumvent the limitations of conventional design of experiment and statistical process control approaches.<sup>[21]</sup> These approaches are highly theoretical, with rare applications limited to small-scale systems.<sup>[22]</sup> Reports of the latest technologies to acquire and interpret the necessary data in an industrial framework are often proprietary know-how which seldom reach the academic world.

The first step of electrode production, slurry manufacturing, is mainly monitored via off-line methods, although the development of innovative continuous mixing techniques has increased the interest for in-line technologies. The electrode slurry is typically sampled at several points during the multistep mixing process and its rheological properties are determined using laboratory rheometers.<sup>[23]</sup> A direct link between the rheology and the electrode performance in cells, beyond the obvious processability requirements, could however not be established in general, with the current running hypothesis of a complex interplay of these features with the coating and drying parameters still to be elucidated.<sup>[24]</sup> Other parameters such as particle size distribution may help understanding the amount of primary to secondary particles (also known as aggregates) in the slurry as well as detect the presence of agglomerates of smaller particles. Conventional optical methods, such as laser diffraction, however, require the dilution and ultrasound-based homogenization of the slurry due to the challenging material (highly concentrated mixtures of solids with extremely low transmission of visible light), therefore hindering a direct measurement.<sup>[25]</sup> Overall, the mixing process is controlled and optimized through heavily relying on experienced operators with mostly off-line tools at their disposal.

Compared to the mixing process, there are established inline technologies for the coating and subsequent drying process that originate from related high-speed roll-to-roll web manufacturing industries. X-ray based methods and ultrasound transmitters are typically used to control the loading of the electrode layer,<sup>[26]</sup> while optical sensors measure the thickness of the dried film before and after calendering.<sup>[13]</sup> High-speed camera systems tuned for visible light detect defects at the surface of the electrode, with new sensors (infrared, X-ray, Raman) continuously in development.<sup>[8,11]</sup> While these systems allow for the main predictor of short-term electrode performance that is electrode loading to be measured precisely and possible deviations (inhomogeneity, defects) to be detected, the quantitative thresholds for significance remains unclear. Failures in the later steps of the battery manufacturing chain or even middle-to-long term degradation effects during battery operation cannot be reliably predicted based on the current state of knowledge. Such findings would allow to better differentiate scrap, standard and premium material and therefore result in significant savings.

### 3. Manufacturing Defects and Their Criticality

Various defects can occur during the production of electrodes for LIBs. In the following, the most important defects and typical causes are briefly described. The types of defects addressed include metal contaminations, point and line defects, as well as inhomogeneities in the composition and microstructure of the electrodes. The description is followed by an overview of the state of the art regarding the criticality of these defects with respect to the influence on the electrochemical performance of electrodes and cells.

#### 3.1. Metal contaminations

Metal contaminations in the electrodes for LIBs originate from contaminated raw materials (e.g., Fe, Co, ...), machine abrasion during mixing, coating, or calendering (e.g., steel, ...) or mechanical processing of the battery components (e.g., Al, Cu, ...). In addition, the increasing use of recycled battery materials could increase the likelihood of unwanted metal contamination, in dissolved or particle form, in electrodes and cells.<sup>[27]</sup> Qian et al.<sup>[28]</sup> investigated cylindrical cells that had failed the quality assurance procedure using X-ray fluorescence (XRF) and detected three kinds of metal impurities: Fe/Cr based impurities from stainless steel, at some defect sites also including additional metals (e.g., Cu and Zn) from the battery manufacturing process and Zr-based particles, most likely from zirconia milling balls (Figure 3a–e). Although these particles in the range of a few microns were detected (cf. Figure 3f), not much information is found on their frequency of occurrence as well as on their actual impact on the electrochemical performance. The authors mention that the investigated cells failed quality assurance due to self-discharge, which suggests the presence of internal (micro-)short-circuits. Impurities located on the surface are especially liable to trigger such an internal short circuit by piercing through the separator (Figure 3g). Another possible failure mechanism is the electrochemical dissolution (oxidation) of metal impurities on the cathode side, followed by redeposition on the anode. In the case of dendritic growth, this can also lead to piercing of the separator and consequently to a short circuit (Figure 3h). Poothikunnath et al. detected a variety of metal impurities in carbon black used as conductive additive in electrodes for LIBs and highlighted the risk that these particles cause the majority of short circuits.<sup>[29]</sup>

Mohanty et al.<sup>[30]</sup> investigated the impact of metal contaminants such as Al foil and Co-powder, which they assumed possible contaminants during electrode production. The contaminants were introduced in quite excessive amounts as foil snippets or powder during the coating process as model samples. The capacity and the coulombic efficiency were found decrease with Co contamination when compared to the baseline case (Figure 3i and k). The authors assign the poor electrochemical performance to metal particles forming alloys with lithium or particles diffusing through the separator and causing a short circuit, which results in a sudden cell failure during 1 C cycling. Al contaminants appear to act less

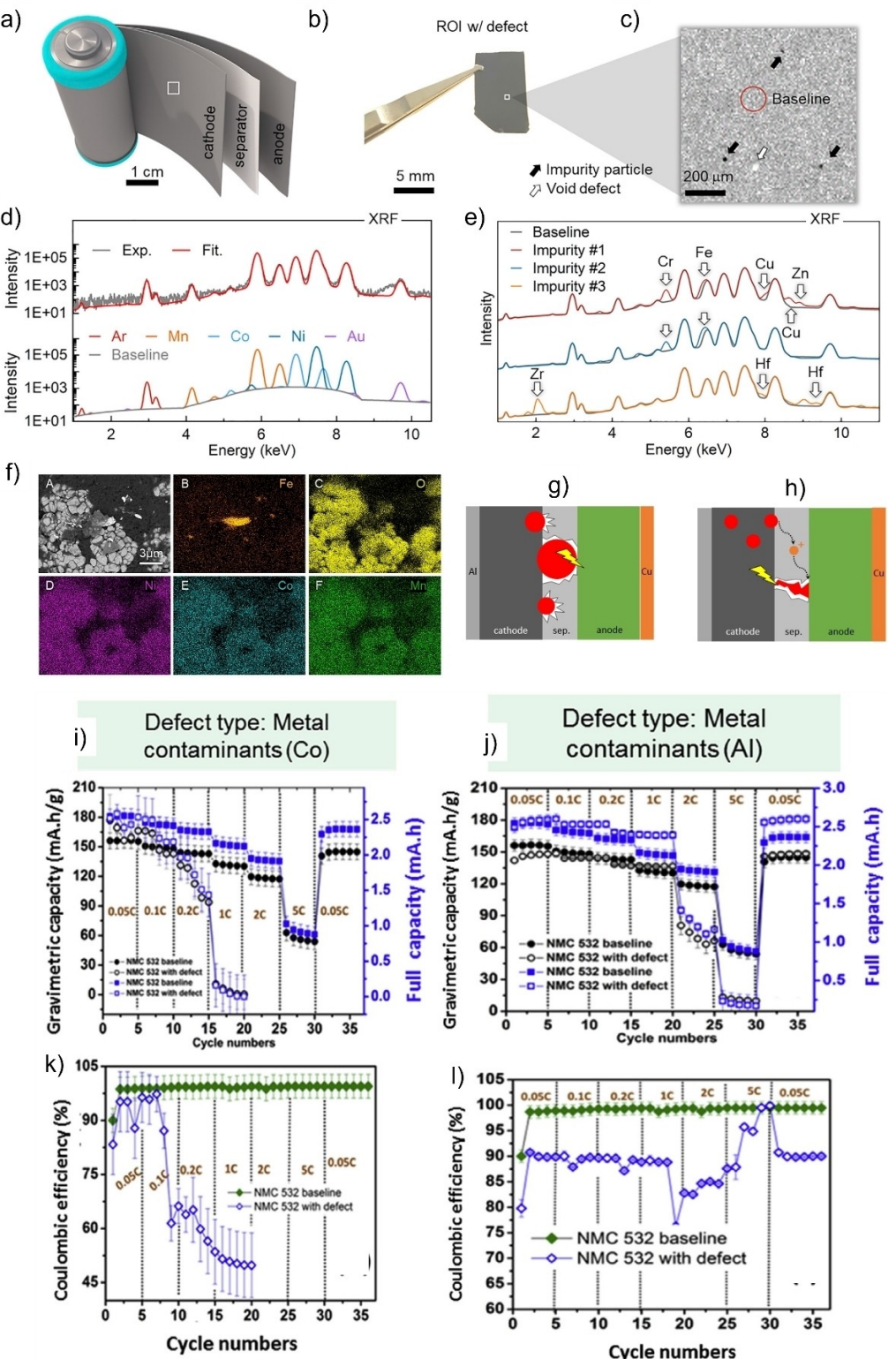


**Figure 3.** a) Representation of the region of interest (ROI) extracted from an 18650-type LIB, b) recovered ROI with defect particles, and c) micro-CT image of (b) showing impurities and void defects. d) and e) XRF analysis of defects with different chemical compositions on the detached cathode. f) SEM image and EDS mappings of the defective regions. Adapted with Permission from Ref. [28]. Copyright (2021) Elsevier. Possible short circuit modes due to metal contaminants: g) metal particle piercing the separator and h) dissolution of metal impurities at the cathode and redeposition at the anode. i–l) Rate capability and coulombic efficiency of NMC532 electrodes with Co powder contaminants (i, k) and Al foil contaminants (j, l) compared the non-contaminated baseline NMC532 electrode. Adapted with Permission from Ref. [30]. Copyright (2016) Elsevier B.V. Published by Elsevier B.V. All rights reserved.

detrimental in regard to capacity, but the coulombic efficiency is strongly depressed to ~90%, indicating the presence of a concurrent electrochemical reactions (Figure 3j and l). The study indicates possible consequences of excessive metal contamination, it does not provide information on tolerance limits, e.g., influence of metal contamination at very low levels, and confirmation of the proposed failure mechanisms is still pending. Fink et al.<sup>[31]</sup> performed a comprehensive study on the influence of metal contaminations in cathodes and anodes on the electrochemical and thermal behavior. Fe, Cu, Al, Mg and Si impurities, i.e., typical residues from the shredding process in the recycling of LIBs, were introduced into electrodes at concentrations of 1 wt%. Iron contaminations in the anode showed a minimal electrochemical influence in half cells. Small irregularities only show up in the first formation cycle, suggesting that the formation of the SEI is disturbed by the reductive passivation of iron, the dissolution of Li<sup>+</sup> into iron-containing surface oxides or a weakly catalytic reaction between the oxidized iron and the electrolyte. In full cells, this leads to a capacity loss. It is suggested that there is an irreversible surface oxidation which may consume the lithium. Al contaminations in the anode showed electrochemical reactivity in half and full cells which originate from alloying with lithium at low potentials.<sup>[32]</sup> Cells with Mg contamination in the anode showed a similar behavior. However, a significant capacity loss can be observed which is interpreted as an irreversible alloying of Li with Mg. In contrast to the other contaminations, Cu contaminations in the anode, not expected to exhibit any reactivity at anode potentials, showed no irregularities during the first cycle of formation but very erratic behavior in the upcoming formation cycles. Some of the full cells surprisingly showed a better capacity than the baseline electrode, which suggests that Cu acts like a conductive additive, increasing the conductivity. Regarding cathode contamination, Fe-containing electrodes showed irregularities in the first cycle of formation and a capacity decay in full cells. It is suggested that the iron has a catalytic role in the electrolyte decomposition. The tests with Al and Mg contamination showed additional oxidation peaks only in the first cycle of formation, which suggests passivation. The Cu contamination showed a capacity decline which later regenerates. It is suggested that Cu oxidizes from Cu<sup>0</sup> to Cu<sup>+</sup> to Cu<sup>2+</sup> allowing Cu ions to be deposited at the anode, which can cause an internal short circuit (cf. Figure 3h) or block pores. For cathodes with Si contamination, it is suggested that, because of the high reactivity of the Si, SiO<sub>2</sub> is formed in reaction with the electrolyte which can then react with Li to Li<sub>2</sub>SiO<sub>3</sub>. For half cells it is unproblematic because there is an infinite Li reservoir. Unlike in full cells, where a capacity decrease is observed due to the lost Li by formation of Li<sub>2</sub>SiO<sub>3</sub>. It should be noted that some of the contaminated cells showed no difference to the baseline electrode, which implies that the particle distribution was irregular, leading to electrodes which do not include metal particle contaminations. These works provide first fundamentals in understanding, which contaminating metals can act detrimentally, but further clarification of their concentration-dependency will be necessary.

### 3.2. Point defects

In the context of electrode manufacturing, point defects are understood as irregularities in surface of the electrode coating of typical length greater than 50 µm, such as pinholes, divots, and blisters. This should not be confused with the term point defects in the sense of a crystallographic irregularity, which are deliberately introduced during material synthesis to improve the electrochemical performance of the active material.<sup>[33]</sup> Point defects in electrode manufacturing can occur due to the bursting of trapped gas bubbles during the drying process.<sup>[30,34]</sup> This can lead to exposure of the current collector and reduction of the local active material loading. Consequently, the N/P ratio, which describes the areal capacity ratio of negative (N) and positive (P) electrode, is varies on the local level, which can lead to overcharging and Li plating. Small differences in local thickness might be leveled during calendering. However, this results into inhomogeneous porosity.

Most studies dealing with point defects focus on detection methods.<sup>[28,35–37]</sup> In addition to elaborate methods such as microcomputer tomography,<sup>[28]</sup> optical systems or infrared (IR) thermography are used to identify point defects. Kapeller et al.<sup>[35]</sup> used a strobed photometric stereo method to detect pinholes (>50 µm diameter) during coating process with a maximum speed of 500 mm s<sup>-1</sup>. Frommknecht et al.<sup>[37]</sup> applied a visual camera in connection with white illumination and a 3D data laser line system in combination with image processing algorithms to detect pinholes. Sharp et al.<sup>[36]</sup> produced bubbles with a diameter of less than one millimeter in the electrode during coating process and detect the defects with flash thermography (Figure 4a). The bubbles show a lower thermal emissivity and can thus be easily detected. Furthermore, the authors<sup>[30,34,36]</sup> show that the thermography is a very suitable method for the detection of various defects besides point defects like line defects, agglomerates, metal contamination and thickness inhomogeneities etc. For example, areas with higher thickness of the electrode show locally increased thermal emission (Figure 4a).

Yang et al.<sup>[38]</sup> investigated Li diffusion around the preintroduced defects in the commercial graphite electrodes using a *situ* optical observation system and numerical simulation (Figure 4b). It is found that gas-filled bubbles slow down Li diffusion compared to defect-free areas, leading to inhomogeneous lithiation. Bubbles in parallel direction reinforce this effect. In contrast, electrolyte-filled bubbles filled lead to faster lithiation because the electrolyte possesses higher diffusivity than graphite. This work<sup>[38]</sup> impressively demonstrates that Li-graphite colorimetry combined with numerical simulation is well suited to determine and understand SOC inhomogeneities resulting from defects.

Mohanty and Ruther et al.<sup>[30,34]</sup> investigated the impact of various artificially introduced point defects on the electrochemical behavior of NCM523. The defects were analyzed by optical images, Li-graphite colorimetry, IR thermography and electrochemical studies. Rate capability and cycling stability were investigated in full-cell configuration against graphite anodes. Electrodes with pinholes show lower capacity than

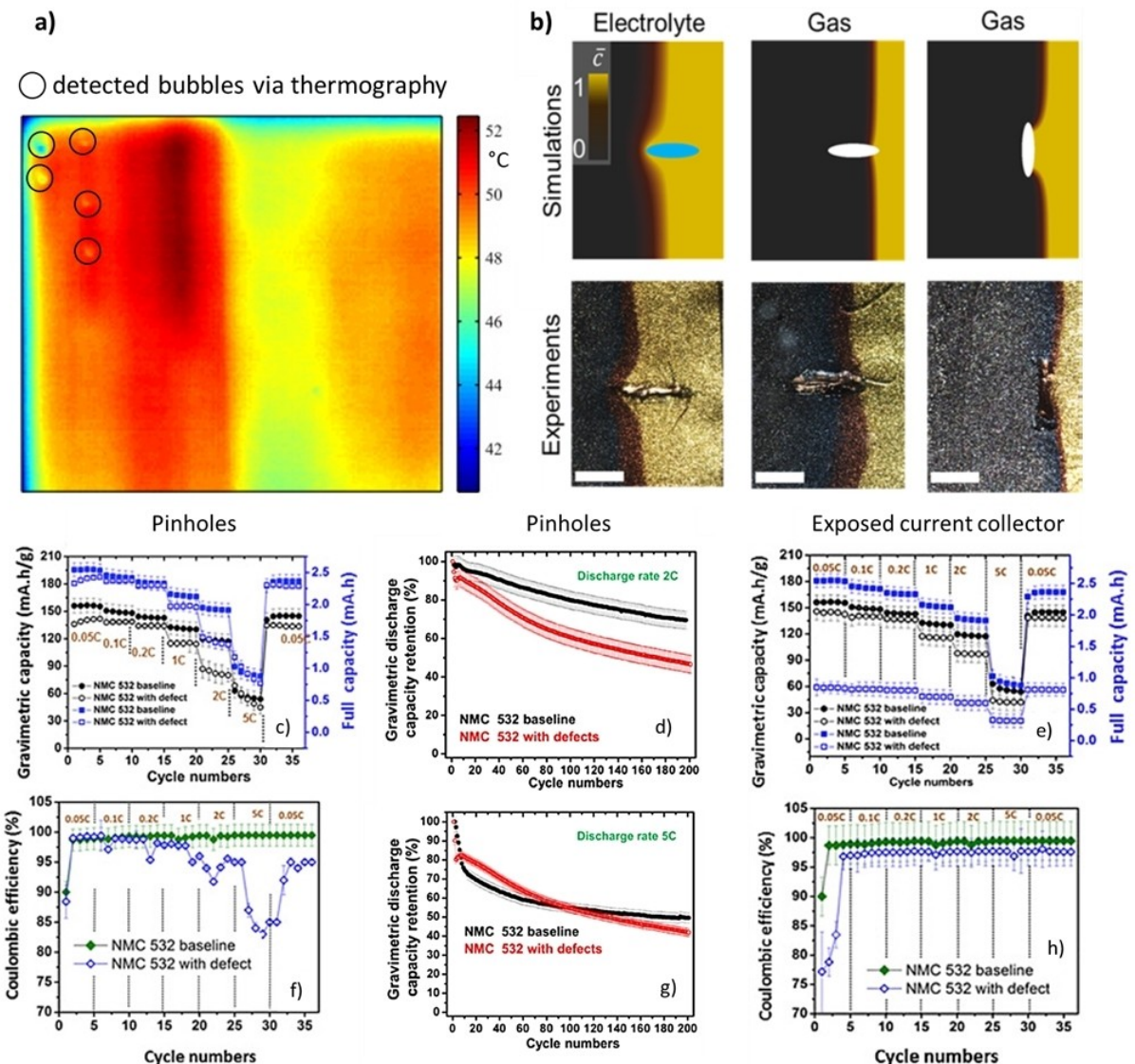


**Figure 4.** a) Detection of bubbles with flash thermography. Adapted with permission from Ref. [36]. Copyright (2014) Elsevier Ltd. All rights reserved.  
 b) Simulated Li concentration maps around the various defects and the corresponding experimental results during lithiation (scale bar is 1 mm). Adapted with permission from Ref. [38]. Copyright (2018) American Chemical Society. c-h) Electrochemical influence of pinholes and exposed current collector in comparison with baseline electrode: c) c-rate test of pinholes, d) cycling performance (2 C) of pinholes, e) c-rate test exposed current collector, f) Coulombic efficiency during c-rate test of pinholes, g) cycling performance (5 C) of pinholes and h) Coulombic efficiency during c-rate test of exposed current collector. Adapted with permission from Ref. [30]. Copyright (2016) Elsevier B.V. Published by Elsevier B.V. All rights reserved.

defect-free electrodes, especially at higher C-rates (Figure 4c). Furthermore, pinholes significantly reduce the coulombic efficiency at higher C-rates (Figure 4f) and lead to decreased capacity retention of 47% @ 2 C and 40% @ 5 C after 200 cycles (Figure 4d and g). In the case of the exposed current collector, the capacity loss is about 10–20% higher compared with the baseline cathode (Figure 4e and h). The full cell capacity shows 60–70% lower capacity, indicating a lower degree of active material in the defective cathode. While these studies indicate the importance of certain point defects in the electrochemical behavior of electrodes and provide useful initial information on the underlying mechanisms, the paucity of data and the lack of variation in defect size, number, and position do not allow us to derive a holistic picture or establish tolerance criteria.

### 3.3. Line defects

Line defects is a broad category which mainly regroups defects that occur in the coating and drying process, since both processes are continuous and linked together in most applications. For example, agglomerates can cause a temporary blockage of the doctor-blade or slot-die resulting in stripe-like defect in the electrode layer. Mohanty et al.<sup>[30]</sup> simulated such a blockage of the slot-die using defined shims with thin (2 mm) and wide (6 mm) inserts, resulting in lines in the web rolling direction devoid of NCM cathode material. The amount of removed material was kept comparable by measuring the performance of electrodes with three thin defects (3X) versus one thick defect (1X), as illustrated in Figure 5(a). The

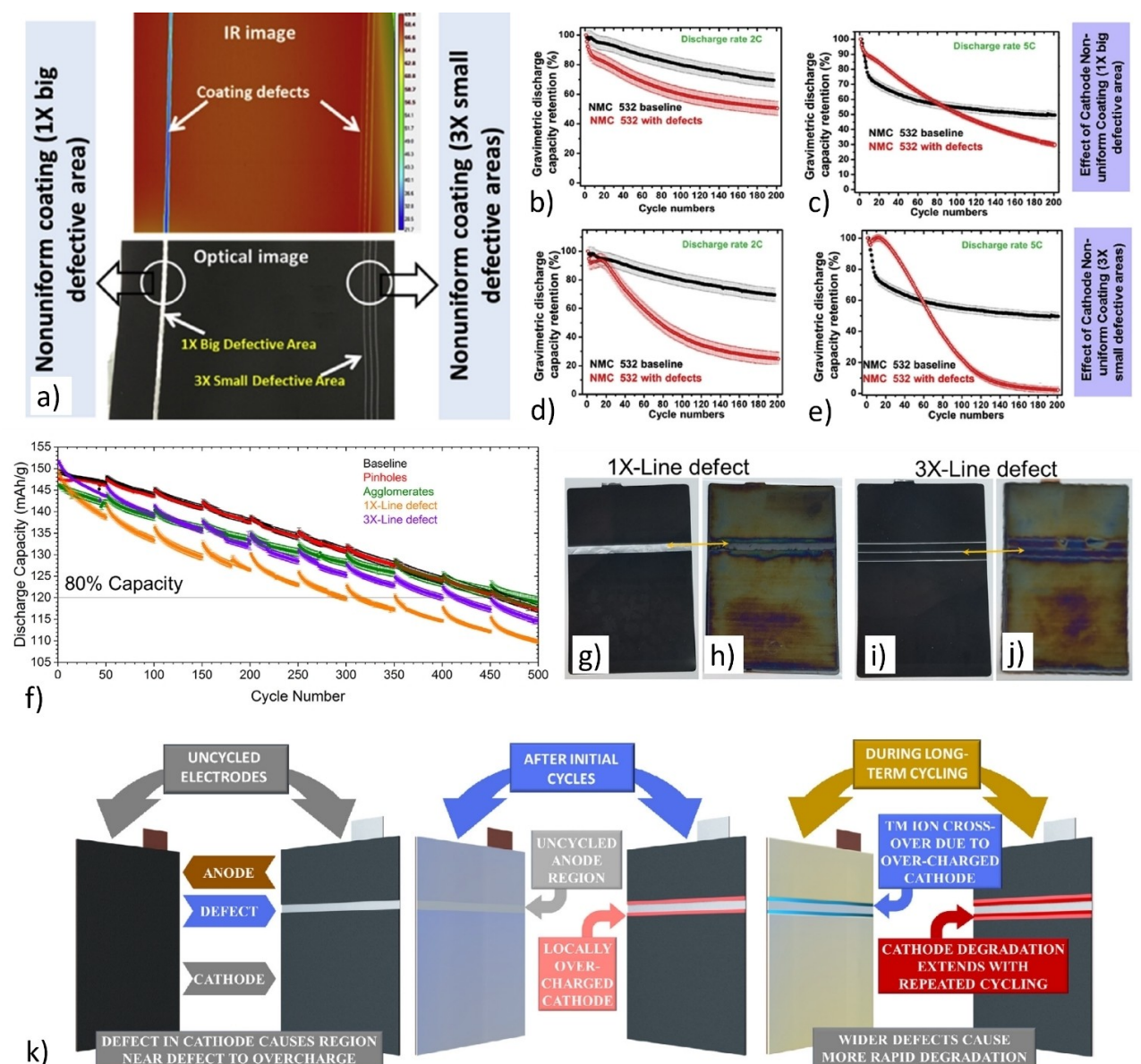


**Figure 5.** a) Visible light and infrared appearance of the provoked line defects; b–e) Capacity fading over 200 cycles under different cycling currents in the case of 1X and 3X defects; Adapted with permission from Ref. [30]. Copyright (2016) Elsevier B.V. Published by Elsevier B.V. All rights reserved. f) Capacity fading of pouch cells with the 1X- and 3X-defects over 500 cycles under 1 C; g–j) Post-mortem appearance of cathode and anode after 500 cycles, with clearly identifiable degraded areas in the anode opposite to the line defects; k) Schematic of the postulated degradation mechanisms in the cell. Adapted with permission from Ref. [34]. Copyright (2018) Elsevier Ltd. All rights reserved.

gravimetric capacity for coin cells with electrodes displaying either defect showed little variation compared to the defect-free cathode in the short term. Long-term cycling (2 C) revealed more drastic effects: Both defects led to a significant capacity fade over 200 cycles, with the 3X-defect especially detrimental with only 20% remaining capacity (versus 45% for the 1X-defect) at the end of the experiment (Figure 5b–e). The faster capacity decline is assigned to the larger interface of the 3X specimens, which could promote delamination during cycling. This claim is supported with SEM images of the specimens with apparent contact loss between electrode material and current collector. The same setup was further investigated by David et al.<sup>[34]</sup> using analytical methods to gain insights in the

degradation process, with larger format pouch cells displaying 1X and 3X-defects. The authors report the cells with 1X-defect as prone to a faster capacity fading compared to 3X-defect, in contradiction with the findings from previous work<sup>[30]</sup> (Figure 5f). The impact of the cell format (coin, pouch) and size relative to the defect size seems therefore to play a decisive role in the subsequent cycling behavior. Post-mortem characterization of the cathode in the 1X-specimen as well as the anode opposite as depicted in Figure 5(g–j) revealed (1) a degradation of the cathode material close to the defect, attributed to local overcharging, (2) a region of uncycled anode material directly opposite to the defect and (3) the migration of transition metals ions from the overcharged cathode region to

the anode opposite. These effects result in the observed capacity loss, which is postulated to be stronger in larger defects due to a higher local distortion of the N/P ratio.

The second main type of reported line defects are cracks of various size, forms and origin, such as inappropriate drying or electrode delamination.<sup>[18,39]</sup> Gao et al. used two-dimensional numerical to determine the impact of crack geometry (parameter  $a$ ,  $b$  and  $\theta$  in Figure 6a) and position (parameter  $d$  in Figure 6a) in the cathode based on the assumption of a blocking effect through imperfect wetting.<sup>[40]</sup> It is found that the specific energy is reduced most significantly in case of long rather than wide cracks that run parallel to and close to the current collector (Figure 6b and c). Specific energy and capacity losses are however limited, with significant degradation only under the assumption of low wetting ratios and high discharge currents densities. Ring-like defects were also simulated with different geometrical configuration and found to have a significant impact on the specific energy of the cell. However, the relevance of this type of cracks in manufactured electrodes was not clearly apparent. Du et al. investigated high-load NMC electrodes with varying degree of cracking based on the solvent composition (NMP, isopropanol and water mixtures).<sup>[41]</sup> Electrodes with similar loading ( $25 \text{ mg cm}^{-2}$ ) were characterized in pouch cells against graphite. The electrodes with the largest cracks showed a higher ohmic resistance of up to 200% and a stronger degradation of the areal capacity over 100 cycles (Figure 6e). Furthermore, the electrodes exhibited a severe capacity loss at higher C-rates, with 50% retention at 1 C and

less than 20% at 2 C (Figure 6f) than the electrode with less or no cracks. Most of these characteristics are attributed to the poor structural integrity of the cracked electrodes, apparent in the photomicrographs of the surface in Figure 6(d).

### 3.4. Inhomogeneities in electrode composition

Compositional inhomogeneities comprise a non-uniform distribution of active material, conductive additive or binder. In case of blended active materials, such as Si-Graphite composites, a non-uniform distribution of the individual components must be considered. As one type of such inhomogeneity, agglomerates are found in electrodes, resulting from insufficient mixing. Mohanty et al. provoked binder and carbon black agglomeration by adjustment of the slurry feed rate, resulting in an overall agglomerate area of  $4.67 \times 105 \mu\text{m}^2$  for a total electrode area of  $1270 \times 105 \mu\text{m}^2$ .<sup>[30]</sup> The position of these agglomerates was identified by IR thermography, as the delayed heat release in the corresponding places results in a local emissivity increase. Surprisingly, a higher rate capability for agglomerate-containing electrodes was observed, however at the cost of lowered coulombic efficiency (~92–97% for the first 35 cycles, compared to ~99% for non-defective electrodes). Consequently, capacity fading in electrodes containing agglomerates occurred more significantly, ending up with as low as 12% of the initial discharge capacity after 200 cycles, as compared to 70% in case of defect-free electrodes. At this point, the

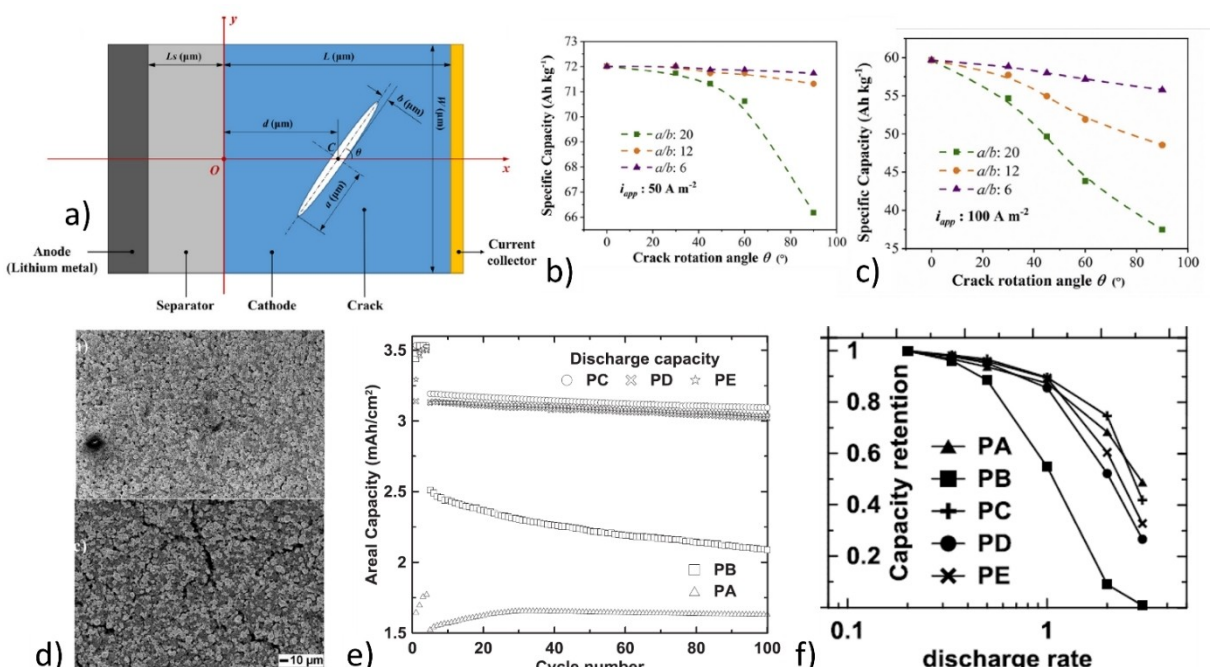


**Figure 6.** a) Schematic of the simulated crack with size and orientation in the cell; b) and c) Specific capacity of the simulated cells for different defect shapes (a/b ratio) and orientation under current densities of  $50 \text{ A m}^{-2}$  and  $100 \text{ A m}^{-2}$ ; Adapted with permission from Ref. [40]. Copyright (2020) Elsevier Ltd. All rights reserved. d) Microscopic view of a cathode ( $25 \text{ mg cm}^{-2}$ ) processed with NMP (top) and with an IPA/water 10/90 wt % solution (bottom). e) Areal capacity of samples with severe (PB) to light (PD) and no cracking (PA, PC, PE) over 100 cycles at C/3. PA has a lower areal capacity due to a lower area loading than the other samples (12.5 vs.  $25 \text{ mg cm}^{-2}$ ); f) Capacity retention in the five samples at different C-rates, normalized to the capacity at C/5. Adapted with permission from Ref. [41]. Copyright (2017) Elsevier B.V. All rights reserved.

underlying reason for this behavior remained unclear. It was however speculated, that large inactive areas result in insufficient electrical connection and low mechanical integrity. In a subsequent study, Wood's group investigated agglomerates, which were deliberately formed by adding active material and conductive additive after the mixing process.<sup>[41]</sup> Contradictory to their earlier work, electrodes containing agglomerates showed an improved long term cycling stability, compared to baseline electrodes. In this case, each electrode of 56 × 84.4 mm contained 15–20 agglomerates each 50–100 µm in size. The authors highlighted the need for further studies on various agglomerates for understanding their effect.

Another case of inhomogeneities in electrode composition is the local variation of active material content. Forouzan et al.<sup>[42]</sup> have simulated different scenarios of locally misbalanced electrodes, i.e., combinations of locally too high-loaded

anodes or cathodes with a locally low-loaded counterpart. In the most detrimental case of low N and high P, the negative electrode is subjected to a higher local current than in case of proper balancing (Figure 7b) and a higher discharge capacity is delivered (Figure 7d). Consequently, the negative electrode locally undergoes a larger SOC change and is therefore utilized more during cycling (Figure 7c). This does not only increase the capacity loss over cycling, but also leads to stronger temperature increase (Figure 7a), elevating degradation at high C-rates, as well as higher risk of Li plating. While incomplete mixing might be the first guess to cause such local active material misbalancing, recent work has shown another source of inhomogeneity. Nikpour et al. revealed that calendering, typically seen as the measure of choice to reduce heterogeneity of an electrode, can lead to aggregation of active material particles.<sup>[43]</sup> Although this leads to a locally increased hetero-

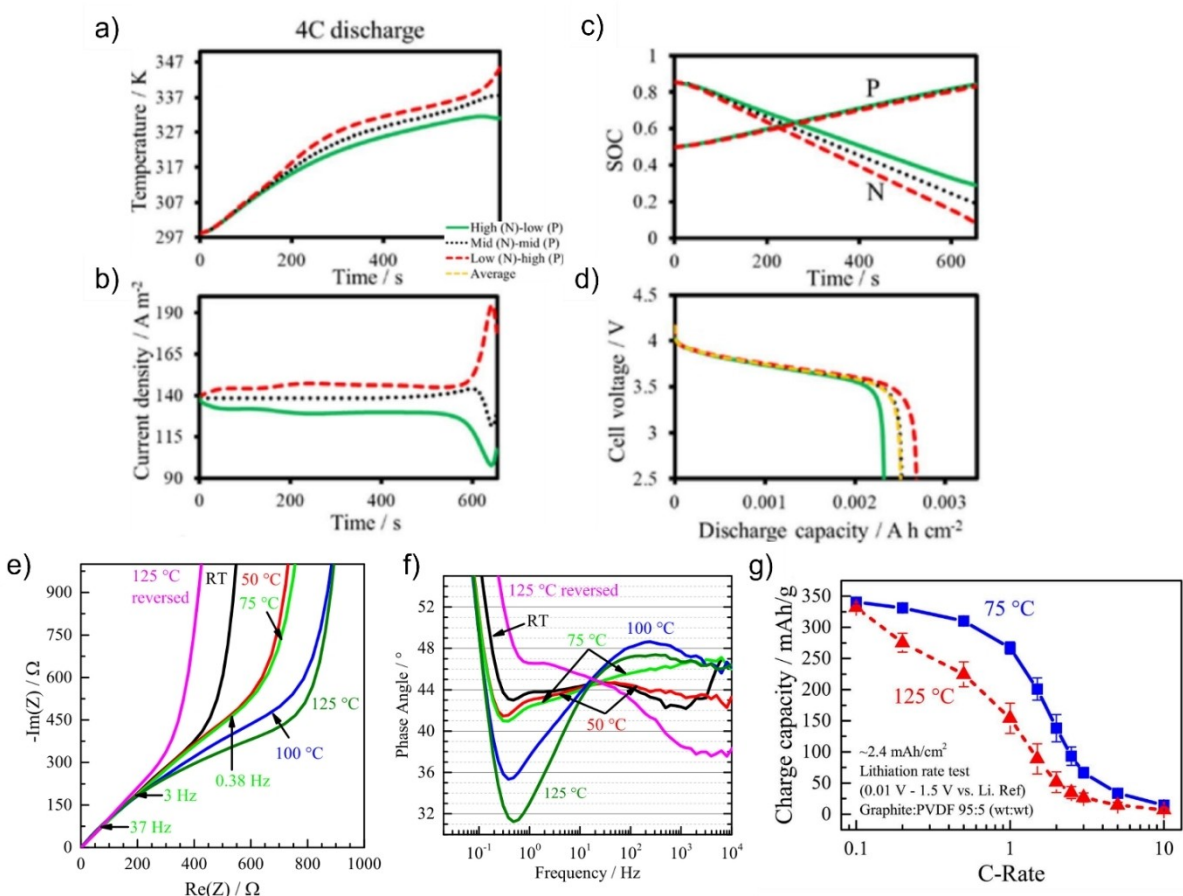


**Figure 7.** a-d) Temperature, current, and positive and negative electrodes states of charge (SOCs) distributions along with discharge curves for the discharging misaligned active material loading case (high-low, middle-middle, and low-high). All regions have similar internal resistances (middle tortuosity and porosity). Notably, the average discharge curves (yellow dashed lines) are weighted averages based on the surface fraction of different spots. The high-low region means the negative electrode with a high active material loading is aligned with the positive electrode with a low active material loading. N and P denote negative and positive electrodes, respectively. Adapted with permission from Ref. [42] under the terms of the Creative Commons Attribution 4.0 License. Copyright (2018) The Author(s). Published by ECS. e-g) Experimental EIS response of graphite electrodes dried between 25 and 125 °C and with a final thickness of ~245 µm ( $\pm$  6%), coated at a wet film thickness of 500 µm; the electrode labeled "125 °C reversed" was dried at 125 °C, removed from the current collector, and re-assembled such that the original CC-side of the electrode becomes the separator-side in the re-assembled cell. EIS measurements (20 mV amplitude, between 10 mHz and 200 kHz) were conducted in a symmetric cell setup (T-cells,  $\phi = 10.95$  mm) using a non-intercalating electrolyte (10 mM TBACIO<sub>4</sub> in EC:EMC 3:7, with  $\kappa = 0.258$  mS/cm). e) High frequency resistance (HFR) corrected Nyquist plots with frequencies marked for the 75 °C sample. f) HFR-corrected phase angle plots. g) Charge (i.e., lithiation) capacity vs. C-rate for cycling the graphite electrodes between 1.5 V and 0.01 V vs. a Li-metal reference electrode. The error bars show the standard deviation of independent measurements with three nominally identical electrodes. Adapted from Ref. [45] under the terms of the Creative Commons CC BY-NC-N license. Copyright (2018) The Author(s). Published by ECS.

genuity in terms of carbon binder domain distribution as well as electronic and ionic conductivity, the beneficial effects of calendering typically outweigh these inhomogeneities.

In addition to agglomerates and local misbalancing, electrodes may exhibit composition inhomogeneity as binder gradients, often originating from fast drying.<sup>[44]</sup> As the solvent is evaporated quickly, binder is transported to the electrode surface and enriching the top layer. Morasch et al. modeled the impedance behavior of different hypothetical scenarios for binder gradients based on either linear or step-wise changes in the ionic resistance along the electrode thickness.<sup>[45]</sup> These transmission line models for blocking conditions resulted in changes of the apparent ion resistance as well as in the evolution of the impedance phase angle. Notably, their model is valid for two-phase systems only, incorporating an active material and binder, but no additional conductive additive. Applying different drying temperatures between room temperature and 125 °C, binder gradients were experimentally generated and confirmed via EDS. The impedance of these electrodes followed the model predictions, i.e., a binder gradient with its maximum at the bottom of the electrode (current collector side) has a lower apparent ionic resistance, while a binder gradient having the maximum on top of the electrode (facing the separator) yields a higher ionic resistance (Figure 7e and f). Based on the bulk electrolyte conductivity and the constant electrode porosity, tortuosity values were determined. For high drying rates (i.e., high temperature and short drying time), the resulting tortuosity was significantly higher than for lower drying rates ( $\tau > 5.5$  for 125 and 100 °C, compared to  $\tau < 3.5$  for room temperature). A rate capability test was carried out in half cells, comparing electrodes dried at 75 and 125 °C (Figure 7g). Both electrodes exhibited similar tortuosity (4.6 for 75 °C compared to 4.4 for 125 °C), but the EIS spectra of the fast-dried electrode pointed at a situation of binder enrichment at the top of the electrode. The resulting inferior rate capability for the electrode dried at 125 °C is hence attributed to a partially pore-blocking binder layer at the surface of the anode. Although the authors point out, that the proposed approach is not suitable to quantify binder gradients, they impressively demonstrate how these gradients influence the electrochemical performance of a cell.

Apart from binder gradients, inhomogeneity may also be present in the distribution of the carbon domain. As it is well known that a ubiquitous carbon distribution is essential for the electrode to provide its full capacity and a satisfactory rate capability, it is likely that inhomogeneities affect these properties. Yari et al. have studied this question by an investigation of model bilayer electrodes, containing layers with varying carbon content.<sup>[46]</sup> They found that, for bilayer electrodes, the rate capability is mainly determined by the bottom layer close to the current collector. While model electrodes with a carbon-depleted bottom layer (Figure 8b) showed inferior properties compared to a single layer electrode, a carbon-enriched bottom layer (Figure 8a) led to superior electrochemical performance. Figure 8(c) illustrates that, in a bilayer system, the bottom layer is mainly responsible for the obtained C-rate (a lower discharge rate-capability coefficient indicates a higher

vulnerability to high C-rates). Using the heterogeneity factor  $\delta$ , describing the mass-averaged relative deviation in the carbon fraction from the mean value, a rise in rate capability is observed when the lower layer is enriched in carbon, while a rate capability decay occurs when the bottom layer is depleted in carbon (Figure 8d). It is therefore important to understand, that inhomogeneity must not be equated to inferior performance and it can rather act destructive or constructive. Interestingly, this trend is also reflected in ageing properties of the electrodes. While carbon-enriched bottom layers enable a better cycling stability than a single layer electrode, carbon-depleted bottom layers lead to a reduced cycle life. The authors speculate that the bad electrical conductivity near the current collector for carbon-depleted bottom layers leads to uneven NMC utilization and therefore current hot spots, which bring about larger diffusion-induced stress as well as a faster local electrolyte decomposition. Additionally, NMC particles may lose connection to the carbon-binder domain, resulting in active material loss and hence capacity fading.

Throughout the last years, blended electrodes using multiple active materials have emerged.<sup>[47]</sup> For such electrodes, particular attention has to be paid to composition inhomogeneities, since the different active materials can have different particle sizes and shapes, making them prone for segregation effects. Etiemble et al. investigated inhomogeneities in NMC/LFP blends using focused ion beam scanning electron microscopy (FIB-SEM) and X-ray tomography.<sup>[48]</sup> When processing either LFP or NMC alone, the rheological properties of the slurries are markedly different. LFP slurries typically need more solvent to avoid mixing inhomogeneities, while NMC slurries are prone to settling if too rich in solvent. In addition, the used materials exhibit strong differences in particle size, amounting to ~100–400 nm for LFP and ~1–20 µm for NMC. X-ray tomography reveals that smaller particles (i.e., a layer of LFP, the smallest NMC fraction and carbon/binder domain) accumulate near the current collector. In NMC-rich electrodes, this leads to a significantly inhomogeneous distribution of NMC particles, while electrodes with high LFP contents do not exhibit these issues. The authors speculate that this rheologically induced segregation will affect the electrical resistance at the electrode-current collector interface. It was moreover found that clusters of LFP as well as NMC-rich zones with higher local porosity occur. While a hard calendering was shown to allow an electrode densification for LFP-rich electrodes, it resulted in NMC particle cracking for the NMC-rich compositions. Although not backed up with electrochemical data it is most likely, that such strong local variations will also locally affect the electrochemical behavior of electrodes.

### 3.5. Microstructural heterogeneity

The rate performance of battery electrodes is significantly affected by the microstructure of the composite layer. The porosity, thickness and tortuosity affect the Li transport in the pore electrolyte, which can limit the attainable capacity at high charge/discharge rates.<sup>[49]</sup> Thus, a certain degree of micro-

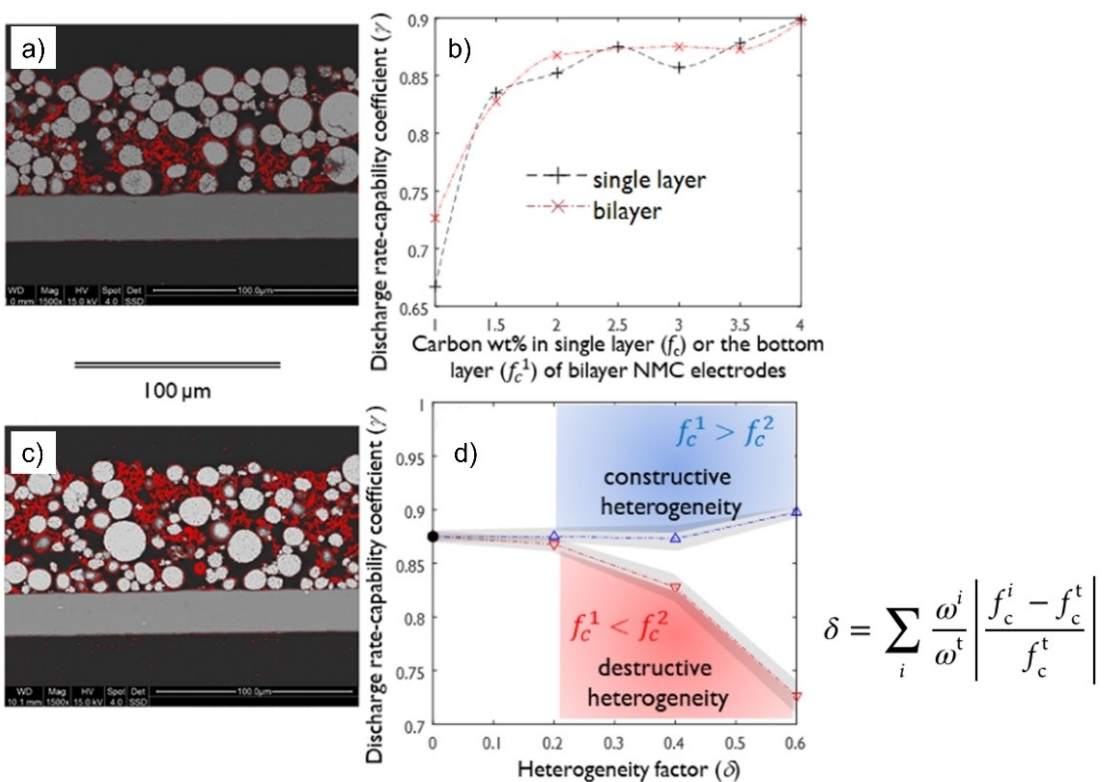


**Figure 8.** Color-enhanced SEM cross-section images of the two bilayer porous electrodes with a) a bottom layer of 4 wt% C ( $f_c^1 = 0.04$ ) and a top layer of 1 wt% C ( $f_c^2 = 0.01$ ); and b) a bottom layer of 1 wt% C and a top layer of 4 wt% C. c) Rate-capability coefficient ( $\gamma$ ) based on the discharge energy in the single-layer (dash) and bilayer (dash-dot) NMC electrodes as a function of carbon content in the single layer and bottom layer, respectively. d) Segregation of the bilayer electrodes in the two groups of constructive (blue zone,  $f_c^1 > f_c^2$ ) and destructive (red zone,  $f_c^1 < f_c^2$ ) heterogeneities based on positive and negative deviations of the rate-capability coefficient from that of the single-layer design. The gray highlighted area represents the uncertainty of the results due to the experimental errors and error propagation. Reproduced with permission from Ref. [46]. Copyright (2020) American Chemical Society.

structural inhomogeneity will affect the electrode performance. Local inhomogeneity can cause uneven utilization of the active material, leading to a reduction in the practical achievable energy density. In addition, the heterogeneity of microstructure leading to non-uniform current, temperature and SOC, and thus non-uniform aging, is believed to be one of the main factors aggravating the degradation of electrodes.<sup>[50,51]</sup> For a given chemistry and application, there is an SOC operating range beyond which capacity loss and permanent damage will occur. Therefore, highly heterogeneous electrodes can cause SOC disparities, resulting in uneven aging of the cell. Lateral gradients of porosity and thickness can lead to an inhomogeneous current density distribution that can affect the counter electrode, e.g., by overlithiation of a graphite anode and subsequent Li-plating.<sup>[52]</sup> Inhomogeneity of electrode porosity, thickness and tortuosity mainly stems from the coating process with unsuitable parameters sets (slurry pressure, slot-die gap, substrate speed) or edge cases that induce an inhomogeneous loading. The local variation in electrode loading translates into local variation in porosity or tortuosity after calendering.<sup>[20]</sup>

While several studies focused the analyses of microstructural heterogeneity by X-ray nano tomography,<sup>[28,53]</sup> the specific influence of variances in porosity, thickness, and tortuosity on the electrochemical performance has scarcely been investigated. Kehrwald et al.<sup>[54]</sup> used numerical simulation to deter-

mine the tortuosity of a commercial 18650 Li-ion cell based on 3D tomography data. The results show a maximum variability of the local tortuosity by a factor of three. In comparison, the porosity of the given electrode is quite homogeneous. Consequently, the tortuosity differences did not result from inhomogeneous active material loading, but most probably from process-related variations during coating or drying. In this work,<sup>[54]</sup> consistent with the work of Harris and Lu,<sup>[50]</sup> it is hypothesized that the heterogeneity has detrimental effects on the performance and lifetime of Li-ion cells because local charge and discharge rates deviate greatly from the mean, leading to local Li plating, SOC inhomogeneity, and reduction of the maximum charge rate. However, quantitative correlations between degree of inhomogeneity and influence on these phenomena are not derived.

Forouzan et al.<sup>[42]</sup> investigated effects of microstructural heterogeneity on the performance and cycle life of a Li-ion cell using a combination of a Newman-type and equivalent circuit models to imitate electrode regions associated with different ionic resistances resulting from heterogeneous tortuosity and porosity. For heterogeneous electrodes (Figure 9a), non-uniformities in temperature, current density, SOC and discharge capacity are observed, which become more evident at higher discharge rates (Figure 9b and c). The initial current density of the high tortuosity and low porosity region is low due to the

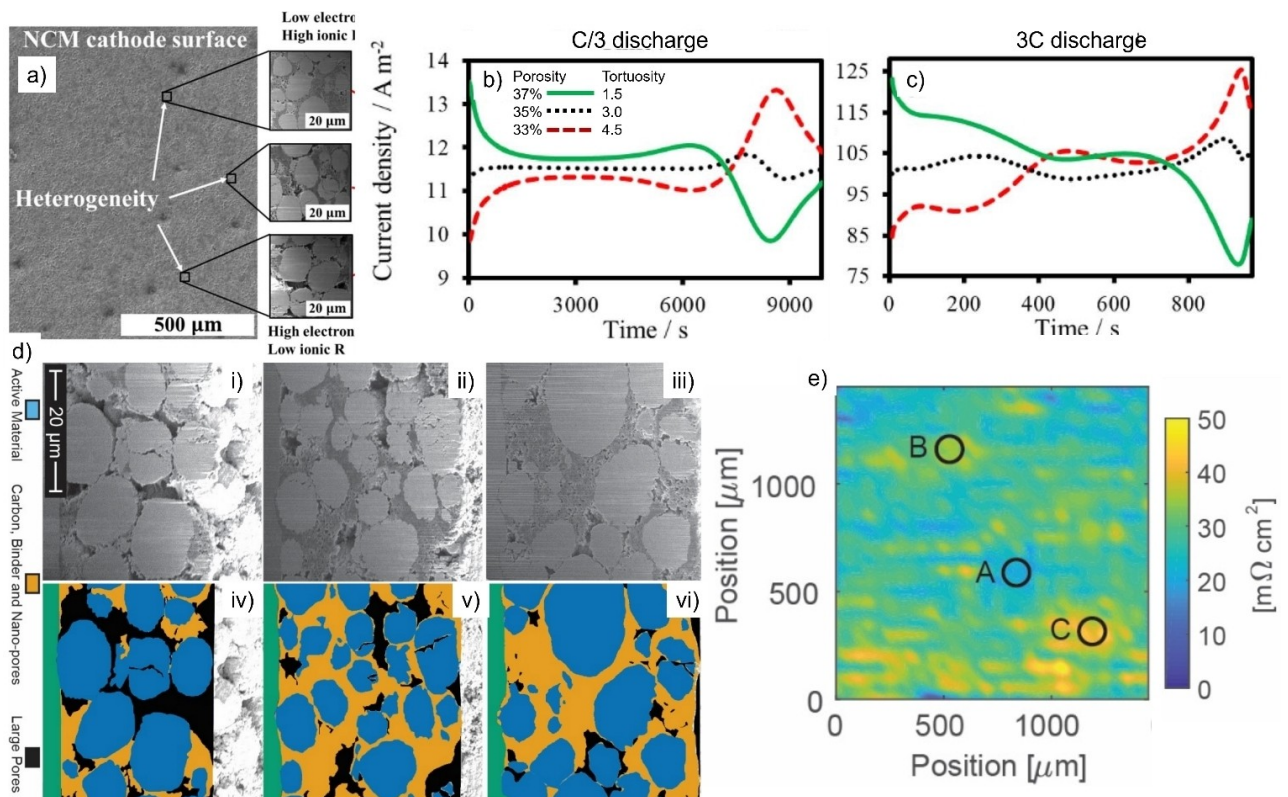


**Figure 9.** a) SEM/FIB images of surfaces and cross-sections of high, medium and low ionic resistance sites of a cathode with NMC active material. Local current density for discharge rates of b) C/3 and c) 3 C at sites of the electrode with different microstructure. Low local porosity and high local tortuosity are associated with high ionic resistances and vice versa. Reproduced with permission from Ref. [42] under the terms of the Creative Commons Attribution 4.0 License. Copyright (2018) The Author(s). Published by ECS. d) SEM images of an NMC cathode with i, iv) high, ii, v) medium and iii, vi) low electronic impedance regions. Panels (i-iii) are the original SEM images and panels (iv-vi) were segmented into 3 regions (active material, CBD, pores) plus current collector. e) Local electronic impedance of an NMC electrode with indication of the low (A), medium (B), and high (C) impedance areas. Reproduced with permission from Ref. [58]. Copyright (2018) Elsevier Ltd. All rights reserved.

high ionic resistance. Due to the different local current density, SOC differences and thus different changes of the equilibrium potential result. Consequently, the current decreases in regions with initial high currents (high porosity, low tortuosity) and increases in regions with initial lower currents (low porosity, high tortuosity). Accordingly, areas with high porosity and low tortuosity degrade more rapidly than those with high tortuosity due to the higher current load, causing a greater loss of capacity when compared to homogenous electrodes. The authors conclude that low heterogeneity of the electrodes is recommended to achieve ultrafast charging with a relatively long lifetime. Quantitative statements on the criticality of individual microstructural parameters are not provided but could probably be determined via comparable simulations for specific electrode combinations. We would like to emphasize that the approach of considering electrodes with different properties connected in parallel, which was used theoretically in the work of Forouzan et al.,<sup>[42]</sup> can also be used for practical investigations to define tolerance limits. Heubner et al. have used such an approach to study internal dynamics,<sup>[55]</sup> local redox behavior,<sup>[56]</sup> and effective electric loads<sup>[57]</sup> in electrodes with blended active materials. A similar experimental approach using electrodes with different microstructure would perfectly complement the theoretical work of Forouzan et al.<sup>[42]</sup> and

would allow straightforward derivation of quantitative tolerance ranges. In a subsequent study of the working group, Vogel et al.<sup>[58]</sup> showed that microstructural heterogeneity (Figure 9d) of commercial quality electrodes strongly influences the resulting local electronic conductivity (Figure 9e). For example, a cathode with active particles  $< 1 \mu\text{m}$  shows impedance variations of 21 to  $41 \text{ m}\Omega \text{cm}^2$  over a distance of 0.5 mm, indicating large variations throughout the film. SEM analyses (Figure 9d) show that the volume fraction of active material is approximately constant, implying that the main source of microstructural heterogeneity is a trade-off between the volume fractions of the carbon binder domain and larger pores. The electronic impedance correlates with the volume fraction of the larger pores and is inversely proportional to the volume fraction of the carbon binder domain.

Lu et al. performed comprehensive analyses on the impact of 3D microstructure design<sup>[59]</sup> of battery electrodes and its evolution during calendering<sup>[60]</sup> using a combination of X-ray CT-based techniques, image-based battery modeling, and electrochemical experiments. The results show that heterogeneous particle and pore phase distribution leads to non-uniform intercalation behavior, resulting in inadequate capacity utilization and lower power density at high rates. Electrodes with graded microstructure significantly improve rate capability

since porosity near the separator largely determines the performance at high rates. In this respect, targeted microstructural inhomogeneities, especially perpendicular to the electrode plane, can also have positive effects on performance. Calendering is found to have opposite effects on thin and thick electrodes. While the volumetric energy density of power-oriented thin electrodes does not benefit due to significant heterogeneity, calendering can improve energy density at moderate rate capability for hybrid applications, and higher calendering is recommended for energy-oriented cells, but at the cost of a severe capacity drop beyond a critical C-rate. The results particularly show that electrodes composed of large particles with broad size distribution exhibit large microstructural heterogeneity, leading to spatial self-assembly during calendering, such as interparticle rotation, non-uniform deformation, and loss of pore interconnectivity. In contrast, electrodes made of small particles are structurally stable with homogeneous deformation and lower pore tortuosity during

calendering. Consequently, calendering aggravates the reaction heterogeneity for electrodes composed of large particles with broad size distribution, leading to underutilization of the active material at high rates, while it does not affect uniform lithiation in electrodes composed of small particles. Analysis of microstructural parameters by Müller et al.<sup>[61]</sup> shows that commercially available graphite anodes exhibit inhomogeneity at different length scales (Figure 10a-f). The magnitude and distribution of particle shape and size is found to affect the homogeneity of porosity, tortuosity and resulting effective transport factor as well as the specific surface area available for the electrochemical reaction on the 100  $\mu\text{m}$  length scale (Figure 10g). Differences in manufacturing can lead to microstructural heterogeneities at centimeter intervals. Electrochemical simulations based on the digitalized microstructures show that electrode microstructural inhomogeneity can lead to different overpotentials in different parts of the electrode (Figure 10h). Comparing homogenous and inhomogeneous

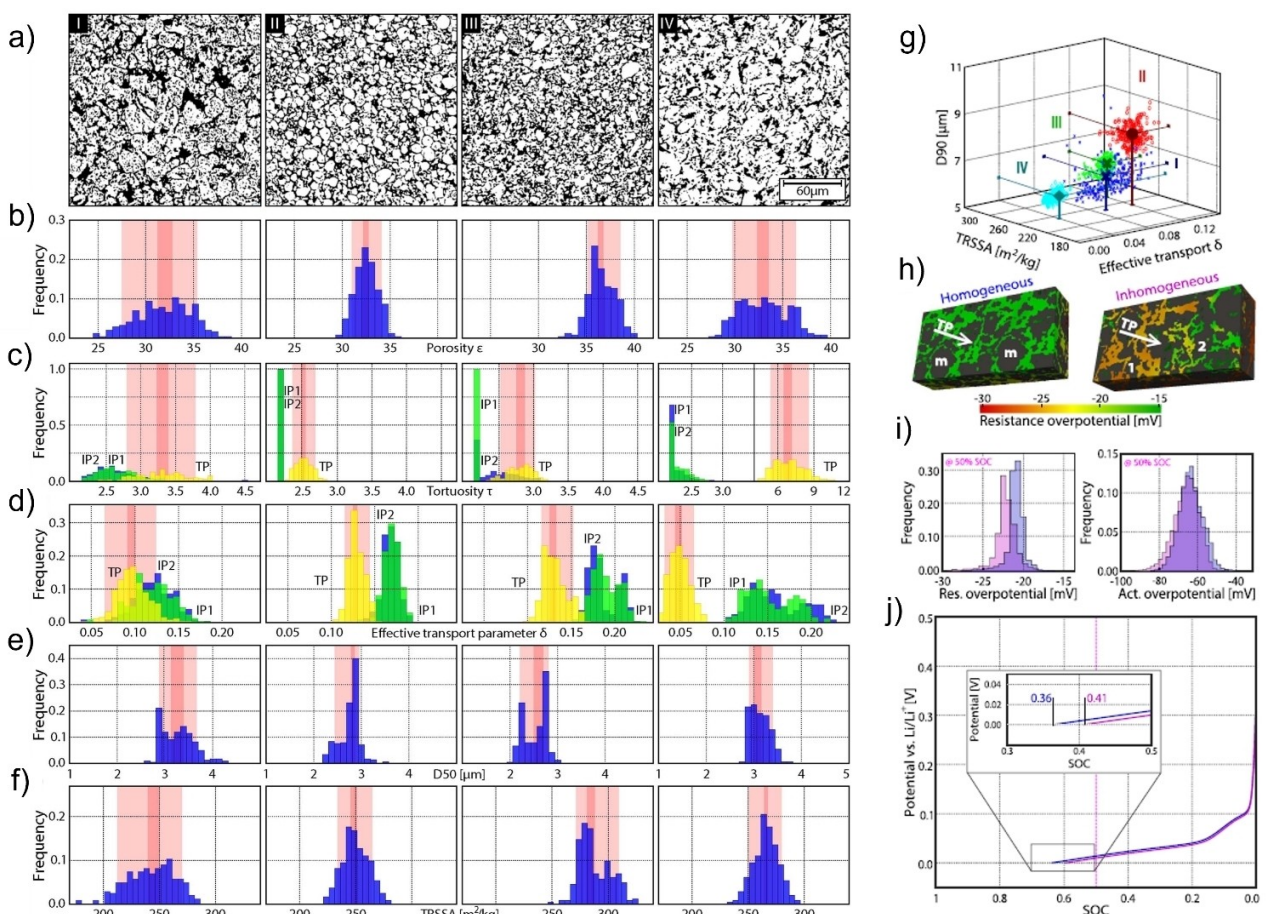


**Figure 10.** a) Sections of binarized tomograms of four different graphite anodes (labeled I, II, III, and IV) found in commercially available LIBs. Corresponding histograms of values for b) porosity, c) tortuosity, d) effective transport parameter, e) particle size (D50 value), and f) tomographically-reconstructed specific surface area (TRSSA). In (c and d), IP1 (green) and IP2 (blue) show the values in the two in-plane (IP) directions, while TP (yellow) shows the values in the through-plane direction. The pink bars represent the 68% interval for a 99% confidence (binomial distribution). The dark pink bars show the median of the interval. g) Scatter plot of microstructural parameter values for electrode I (blue "x"), II (red "o"), III (green "+"), and IV (cyan triangles). h) Distribution of the resistance overpotential in the electrolyte of a homogeneous electrode and an inhomogeneous electrode at SOC = 50% during a 1 C charge. i) The resistance and activation overpotentials at SOC = 50% shown in bar plots in blue for the homogeneous structure and pink for the inhomogeneous structure. j) Potential curves of the homogeneous (blue) and inhomogeneous (pink) microstructures during 1 C charging. Reproduced with permission from Ref. [61] under the terms of the Creative Commons Attribution 4.0 License. Copyright (2018) The Author(s). Published by ECS.

electrodes confirms that the inhomogeneous structure has higher overpotential at the same C-rate (Figure 10i and j), even though the effective transport parameter is slightly lower for the homogeneous structure.

The above results have been confirmed by further simulation studies.<sup>[62]</sup> In contrast, experimental work to directly derive tolerance criteria for microstructural heterogeneity has not yet been performed. The simulations can predict well the electrochemical performance of electrodes and cells, e.g., rate capability. However, it is difficult to estimate effects of the type and extent of microstructural heterogeneity on cycling stability and any safety risks. This is a knowledge gap that we believe needs to be urgently addressed to develop efficient and intelligent inline monitoring tools and reduce scrap rates in electrode and battery cell production.

#### 4. Conclusions and Perspectives

Various defects can occur during the production of electrodes for LIBs, including metal contaminations, point and line defects, as well as inhomogeneities in the composition and micro-

structure of the electrodes. Although corresponding failure mechanisms in the cell for these different defect types are occasionally reported (Figure 11), no comprehensive assessment of defect criticality has yet been conducted.

Metal contaminations introduced by raw materials or during electrode manufacturing have a significant impact on battery performance and safety. Depending on the size, concentration and type of metal, the capacity retention decreases and short circuits can occur within the cell. The additional reactions occurring according to the type of metal contamination as well as the influence of concentration and particle size on battery performance are currently still insufficiently understood, which makes it difficult to derive quantitative criticality criteria. Point defects, such as pinholes, divots, and blisters, have a negative impact on the capacity, rate capability as well as cycling stability of LIB and can lead to inhomogeneous lithiation and delithiation. In the future, the electrochemical influence of the different point defects in terms of their size, number and position in the electrode should also be investigated to deduce at what point a negative influence on the battery performance can be expected. Line defects, typically due to inappropriate processing parameters, can have

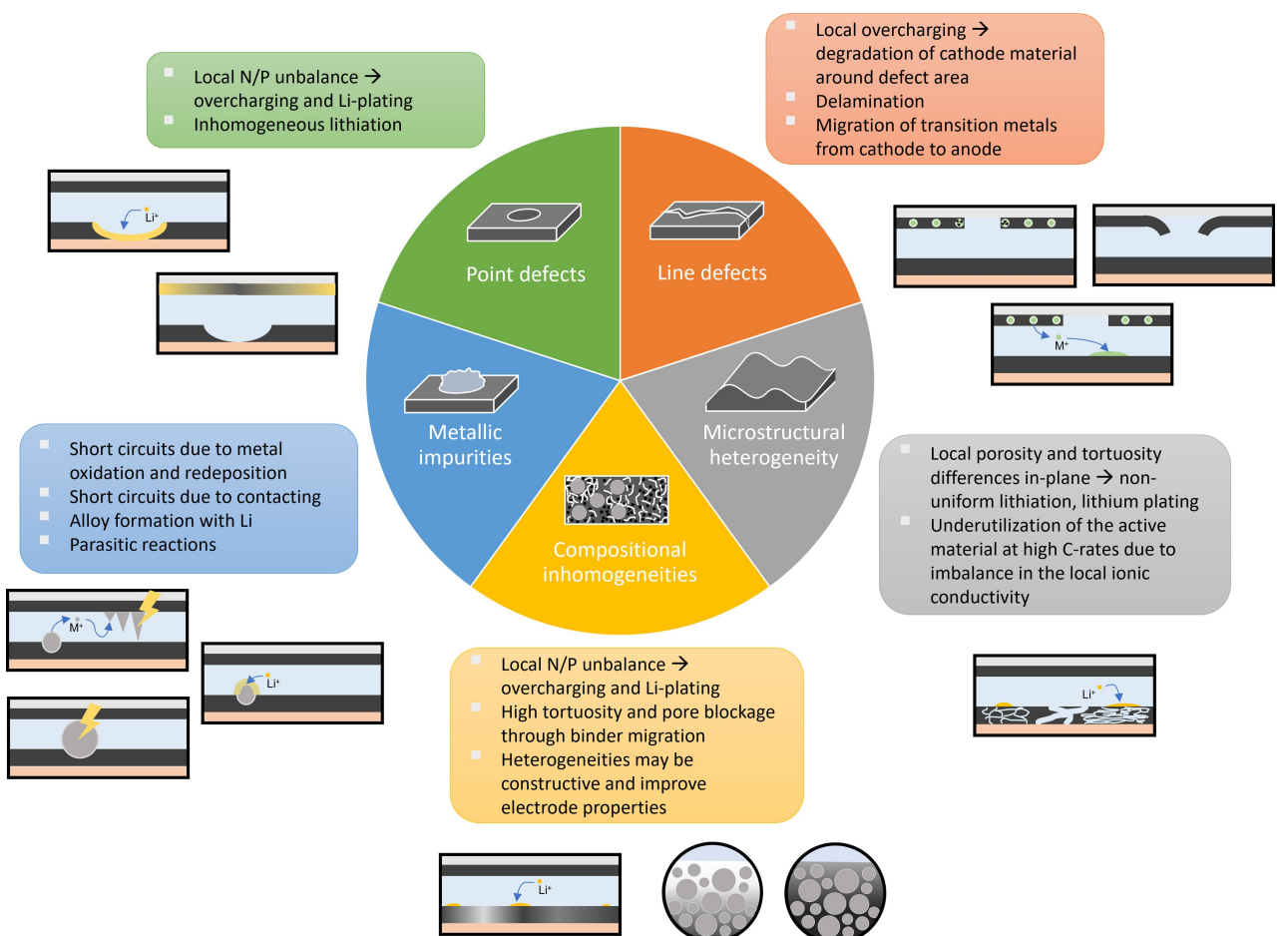


**Figure 11.** Overview of the five reviewed defect types with the associated mechanisms that influence the electrochemical performance of corresponding cells. The mechanism diagrams depict an idealized single layer cell with an anode versus cathode configuration. The circular inserts depict simplified binder and conductive additive gradients perpendicular to the current collector.

negligible to severe effects on battery performance. The impact of line defects appears to be highly dependent not only on defect size and shape, but also on cell format. Although some explanations for corresponding degradation mechanism have been proposed, only very specific cases have been studied experimentally. Further research efforts need to broaden the range of materials and cell formats studied and systematically vary the shape and size of the line defects (width, depth, orientation) investigated to reach meaningful conclusions regarding critical thresholds for quality assurance. The occurrence of agglomerates is still quite poorly understood in terms of its influence on electrochemical behavior, and systematic studies of the various types and degrees of agglomeration will be inevitable to shed light on this issue. Binder gradients, often resulting from drying, increase the impedance and reduce the rate capability of electrodes. For electrodes with blended active materials, special attention must be paid to rheologically induced segregation if the different materials have different particle size, shape or density. In all cases, further work is required to determine quantitative thresholds of defects and inhomogeneities that are still acceptable. While several studies have focused on the quantitative analysis of microstructural heterogeneity, the criticality of porosity, thickness, and tortuosity inhomogeneity has hardly been investigated experimentally. By understanding how distributions of particle size and shape form or slurry and electrode processing cause microstructural inhomogeneity and affect performance, it is possible to determine the extent to which homogeneity should be a priority for certain applications and how homogeneity can be achieved through intelligent material selection and processing. In this context, it should be emphasized that irregularities in the electrode coating do not necessarily have to have negative impact on the electrochemical performance. For example, certain gradients of electrical and ionic conductivity along the thickness of the electrode (through-plane) lead to an improvement in electrochemical performance, while in-plane inhomogeneities lead to a decrease in rate capability and cycling stability. Classification by constructive and destructive defects and corresponding relationships between electrode design and electrochemical performance need to be studied and understood more deeply in the future to establish guidelines on how to design electrodes by regulating electrode defects to improve battery performance.

In general, the criticality of defects arising during electrode manufacturing has been little studied to date. Most of the existing research reports focus on the impact of defects on the electrochemical performance of the cells. In comparison, concrete effects of defects on safety, which in a broader sense is also part of the cell's performance,<sup>[63]</sup> are hardly studied and understood. However, from our point of view, it is critical to know what levels of contamination, coating defects, compositional, and microstructural heterogeneity are acceptable for adequate electrochemical performance, safety, and long-term stability to optimize the electrode fabrication process for a trade-off between quality and cost. To close this knowledge gap, advanced experimental methods must be developed and corresponding systematic studies need to be conducted. This

requires not only post-mortem examinations on a laboratory scale, but also non-invasive detection methods. Optical and acoustic-based methods in combination with data evaluation using artificial intelligence appear promising in this direction.<sup>[9,64]</sup> This could also make it possible to make defect evaluation more universal instead of depending on format/size/capacity/material. Finally, this will be the basis for selecting or developing appropriate inline quality assurance methods for electrode manufacturing. The detection limits of the methods must be suitable to detect critical defect types, sizes and concentrations. At the same time, data acquisition and processing must be fast enough to adjust the process conditions in time or to mark faulty electrode areas with the aim of significantly reducing scrap rates, increasing safety and making battery production more efficient and sustainable.

## Acknowledgements

This work was supported by the German Federal Ministry of Education and Research (BMBF) in the framework of Battery Competence Cluster AQua via the projects KritBatt (Grant No. 03XP0360A, 03XP0360B) and IQ-EI (Grant No. 03XP0359D). Open Access funding enabled and organized by Projekt DEAL.

## Conflict of Interest

The authors declare no conflict of interest.

**Keywords:** criticality · defects · electrode manufacturing · lithium-ion batteries

- [1] A. Masias, J. Marcicki, W. A. Paxton, *ACS Energy Lett.* **2021**, *6*, 621–630.
- [2] a) M. Armand, P. Axmann, D. Bresser, M. Copley, K. Edström, C. Ekberg, D. Guyomard, B. Lestriez, P. Novák, M. Petranikova, W. Porcher, S. Trabesinger, M. Wohlfahrt-Mehrens, H. Zhang, *J. Power Sources* **2020**, *479*, 228708; b) M. Li, J. Lu, Z. Chen, K. Amine, *Adv. Mater.* **2018**, *30*, 1800561; c) J. Xie, Y.-C. Lu, *Nat. Commun.* **2020**, *11*, 2499.
- [3] a) X. Zeng, M. Li, D. Abd El-Hady, W. Alshitari, A. S. Al-Bogami, J. Lu, K. Amine, *Adv. Energy Mater.* **2019**, *9*, 1900161; b) A. Eftekhari, *ACS Sustainable Chem. Eng.* **2019**, *7*, 5602–5613.
- [4] C. Xu, Q. Dai, L. Gaines, M. Hu, A. Tukker, B. Steubing, *Commun. Mater.* **2020**, *1*, 99.
- [5] L. Gaines, Q. Dai, J. T. Vaughney, S. Gillard, *Recycling* **2021**, *6*, 31.
- [6] L. Brückner, J. Frank, T. Elwert, *Metals* **2020**, *10*, 1107.
- [7] a) F. Duffner, L. Mauler, M. Wentker, J. Leker, M. Winter, *Int. J. Prod. Econ.* **2021**, *232*, 107982; b) I.-Y. L. Hsieh, M. S. Pan, Y.-M. Chiang, W. H. Green, *Appl. Energy* **2019**, *239*, 218–224.
- [8] J.-C. Panitz, P. Novák, *J. Power Sources* **2001**, *97–98*, 174–180.
- [9] L. P. Bauermann, L. V. Mesquita, C. Bischoff, M. Drews, O. Fitz, A. Heuer, D. Biro, *J. Power Sources* **2020**, *6*, 100035.
- [10] J. Xu, Y. Liu, H. Xie, F. Luo, *IEEE Trans. Instrum. Meas.* **2020**, *69*, 3157–3169.
- [11] A. Etiemble, N. Besnard, J. Adrien, P. Tran-Van, L. Gautier, B. Lestriez, E. Maire, *J. Power Sources* **2015**, *298*, 285–291.
- [12] A. Kwade, W. Haselrieder, R. Leithoff, A. Modlinger, F. Dietrich, K. Droeder, *Nat. Energy* **2018**, *3*, 290–300.
- [13] R. Korthauer, *Handbuch Lithium-Ionen-Batterien*, Springer Berlin Heidelberg, Berlin, Germany, 2013.
- [14] Y. Liu, R. Zhang, J. Wang, Y. Wang, *iScience* **2021**, *24*, 102332.
- [15] J. C. Flynn, C. Marsh, in *Proceedings of the Thirty-Second Intersociety Energy Conversion Engineering Conference*. July 27 - August 1, 1997,

- Honolulu, Hawaii (Ed.: E. J. Cairns), American Institute of Chemical Engineers, New York, NY, 1997.
- [16] S. Spiegel, T. Heckmann, A. Altvater, R. Diehm, P. Scharfer, W. Schabel, *J. Coat. Technol. Res.* **2021**, *19*, 121–130.
- [17] a) S. Jaiser, M. Müller, M. Baunach, W. Bauer, P. Scharfer, W. Schabel, *J. Power Sources* **2016**, *318*, 210–219; b) J. Chen, J. Liu, Y. Qi, T. Sun, X. Li, *J. Electrochim. Soc.* **2013**, *160*, A1502–A1509.
- [18] J. Kumberg, M. Müller, R. Diehm, S. Spiegel, C. Wachsmann, W. Bauer, P. Scharfer, W. Schabel, *Energy Technol.* **2019**, *7*, 1900722.
- [19] M. J. Lain, J. Brandon, E. Kendrick, *Batteries* **2019**, *5*, 64.
- [20] T. Günther, D. Schreiner, A. Metkar, C. Meyer, A. Kwade, G. Reinhart, *Energy Technol.* **2020**, *8*, 1900026.
- [21] a) J. Schnell, G. Reinhart, *Procedia CIRP* **2016**, *57*, 568–573; b) T. Kornas, E. Knak, R. Daub, U. Bührer, C. Lienemann, H. Heimes, A. Kampker, S. Thiede, C. Herrmann, *Procedia CIRP* **2019**, *81*, 75–80; c) J. Wanner, M. Weeber, K. P. Birke, A. Sauer, in *2019 9th International Electric Drives Production Conference (EDPC)*, IEEE, 2019.
- [22] A. Turetskyy, J. Wessel, C. Herrmann, S. Thiede, *Procedia CIRP* **2020**, *93*, 168–173.
- [23] W. B. Hawley, J. Li, *J. Energy Storage* **2019**, *25*, 100862.
- [24] B. Bitsch, J. Dittmann, M. Schmitt, P. Scharfer, W. Schabel, N. Willenbacher, *J. Power Sources* **2014**, *265*, 81–90.
- [25] H. Dreger, M. Huelsebrock, L. Froboese, A. Kwade, *Ind. Eng. Chem. Res.* **2017**, *56*, 2466–2474.
- [26] C. D. Reynolds, P. R. Slater, S. D. Hare, M. J. Simmons, E. Kendrick, *Materials Design* **2021**, *209*, 109971.
- [27] P. Ardia, S. Stallone, D. Cericola, *Talanta* **2021**, *224*, 121827.
- [28] G. Qian, F. Monaco, D. Meng, S.-J. Lee, G. Zan, J. Li, D. Karpov, S. Gul, D. Vine, B. Stripe, J. Zhang, J.-S. Lee, Z.-F. Ma, W. Yun, P. Pianetta, X. Yu, L. Li, P. Cloeten, Y. Liu, *Cell Rep. Phys. Sci.* **2021**, *2*, 100554.
- [29] A. Poozhikunnath, J. Favata, B. Ahmadi, J. Xiong, L. Bonville, S. Shahbazmohamadi, J. Jankovic, R. Maric, *J. Electrochim. Soc.* **2019**, *166*, A3335–A3341.
- [30] D. Mohanty, E. Hockaday, J. Li, D. K. Hensley, C. Daniel, D. L. Wood, *J. Power Sources* **2016**, *312*, 70–79.
- [31] K. E. Fink, B. J. Polzin, J. T. Vaughay, J. J. Major, A. R. Dunlop, S. E. Trask, G. T. Jeka, J. S. Spangenberger, M. A. Keyser, *J. Power Sources* **2022**, *518*, 230760.
- [32] H. Wang, H. Tan, X. Luo, H. Wang, T. Ma, M. Lv, X. Song, S. Jin, X. Chang, X. Li, *J. Mater. Chem. A* **2020**, *8*, 25649–25662.
- [33] a) Z. Yang, F. Lin, *J. Phys. Chem. C* **2021**, *125*, 9618–9629; b) Y. Zhang, L. Tao, C. Xie, D. Wang, Y. Zou, R. Chen, Y. Wang, C. Jia, S. Wang, *Adv. Mater.* **2020**, *32*, 1905923.
- [34] L. David, R. E. Ruther, D. Mohanty, H. M. Meyer, Y. Sheng, S. Kalnaus, C. Daniel, D. L. Wood, *Appl. Energy* **2018**, *231*, 446–455.
- [35] C. Kapeller, B. Blaschitz, E. Bodenstorfer, in *Forum Bildverarbeitung 2020* (Eds.: M. Heizmann, T. Längle), Karlsruhe Institute of Technology, Karlsruhe, Germany, 2020.
- [36] N. Sharp, P. O'Regan, D. Adams, J. Caruthers, A. David, M. Suchomel, *NDT&E Int.* **2014**, *64*, 41–51.
- [37] A. Frommknecht, M. Schmauder, L. Boonen, C. Glanz, in *Optical Measurement Systems for Industrial Inspection XI* (Eds.: P. Lehmann, W. Osten, A. Albertazzi Gonçalves), SPIE, 2019.
- [38] L. Yang, H.-S. Chen, W.-L. Song, D. Fang, *ACS Appl. Mater. Interfaces* **2018**, *10*, 43623–43630.
- [39] B. Lu, C. Ning, D. Shi, Y. Zhao, J. Zhang, *Chinese Phys. B* **2020**, *29*, 26201.
- [40] T. Gao, A. Kim, W. Lu, *Electrochim. Acta* **2020**, *363*, 137197.
- [41] Z. Du, K. M. Rollag, J. Li, S. J. An, M. Wood, Y. Sheng, P. P. Mukherjee, C. Daniel, D. L. Wood, *J. Power Sources* **2017**, *354*, 200–206.
- [42] M. M. Forouzan, B. A. Mazzeo, D. R. Wheeler, *J. Electrochim. Soc.* **2018**, *165*, A2127–A2144.
- [43] M. Nikpour, N. Barrett, Z. Hillman, A. I. Thompson, B. A. Mazzeo, D. R. Wheeler, *J. Electrochim. Soc.* **2021**, *168*, 60547.
- [44] J. Seeba, S. Reuber, C. Heubner, A. Müller-Köhne, M. Wolter, A. Michaelis, *Chem. Eng. J.* **2020**, *402*, 125551.
- [45] R. Morasch, J. Landesfeind, B. Suthar, H. A. Gasteiger, *J. Electrochim. Soc.* **2018**, *165*, A3459–A3467.
- [46] S. Yari, H. Hamed, J. D'Haen, M. K. van Bael, F. U. Renner, an Hardy, M. Safari, *ACS Appl. Energ. Mater.* **2020**, *3*, 11820–11829.
- [47] C. Heubner, T. Liebmann, M. Schneider, A. Michaelis, *Electrochim. Acta* **2018**, *269*, 745–760.
- [48] A. Etienne, N. Besnard, A. Bonnin, J. Adrien, T. Douillard, P. Tran-Van, L. Gautier, J.-C. Badot, E. Maire, B. Lestriez, *J. Mater. Sci.* **2017**, *52*, 3576–3596.
- [49] C. Heubner, M. Schneider, A. Michaelis, *Adv. Energy Mater.* **2020**, *10*, 1902523.
- [50] S. J. Harris, P. Lu, *J. Phys. Chem. C* **2013**, *117*, 6481–6492.
- [51] X. Zhu, R. I. Revilla, J. Jaguement, J. van Mierlo, A. Hubin, *J. Phys. Chem. C* **2019**, *123*, 30046–30058.
- [52] A. W. Abboud, E. J. Dufek, B. Liaw, *J. Electrochim. Soc.* **2019**, *166*, A667–A669.
- [53] a) V. Shapovalov, K. Kutukova, S. Maletti, C. Heubner, V. Butova, I. Shukava, A. Guda, A. Soldatov, E. Zschech, *Crystals* **2022**, *12*, 3; b) H. Liu, S. Kazemiabnabi, A. Grenier, G. Vaughan, M. Di Michiel, B. J. Polzin, K. Thornton, K. W. Chapman, P. J. Chupas, *ACS Appl. Mater. Interfaces* **2019**, *11*, 18386–18394.
- [54] D. Kehrwald, P. R. Shearing, N. P. Brandon, P. K. Sinha, S. J. Harris, *J. Electrochim. Soc.* **2011**, *158*, A1393–A1399.
- [55] C. Heubner, T. Liebmann, C. Lämmel, M. Schneider, A. Michaelis, *J. Energy Storage* **2018**, *20*, 101–108.
- [56] C. Heubner, T. Liebmann, C. Lämmel, M. Schneider, A. Michaelis, *ChemElectroChem* **2018**, *5*, 425–428.
- [57] T. Liebmann, C. Heubner, C. Lämmel, M. Schneider, A. Michaelis, *ChemElectroChem* **2019**, *6*, 5728–5734.
- [58] J. E. Vogel, M. M. Forouzan, E. E. Hardy, S. T. Crawford, D. R. Wheeler, B. A. Mazzeo, *Electrochim. Acta* **2019**, *297*, 820–825.
- [59] X. Lu, A. Bertei, D. P. Finegan, C. Tan, S. R. Daemi, J. S. Weaving, K. B. O'Regan, T. M. M. Heenan, G. Hinds, E. Kendrick, D. J. L. Brett, P. R. Shearing, *Nat. Commun.* **2020**, *11*, 2079.
- [60] X. Lu, S. R. Daemi, A. Bertei, M. D. Kok, K. B. O'Regan, L. Rasha, J. Park, G. Hinds, E. Kendrick, D. J. Brett, P. R. Shearing, *Joule* **2020**, *4*, 2746–2768.
- [61] S. Müller, J. Eller, M. Ebner, C. Burns, J. Dahn, V. Wood, *J. Electrochim. Soc.* **2018**, *165*, A339–A344.
- [62] A. Rucci, A. C. Ngandjong, E. N. Primo, M. Maiza, A. A. Franco, *Electrochim. Acta* **2019**, *312*, 168–178.
- [63] a) Y. Jia, B. Liu, Z. Hong, S. Yin, D. P. Finegan, J. Xu, *J. Mater. Chem. A* **2020**, *8*, 12472–12484; b) B. Liu, Y. Jia, J. Li, S. Yin, C. Yuan, Z. Hu, L. Wang, Y. Li, J. Xu, *J. Mater. Chem. A* **2018**, *6*, 21475–21484; c) Q. Wu, Le Yang, N. Li, Y. Chen, Q. Wang, W.-L. Song, X. Feng, Y. Wei, H.-S. Chen, *J. Power Sources* **2022**, *540*, 231602.
- [64] J. B. Robinson, R. E. Owen, M. D. R. Kok, M. Maier, J. Majasan, M. Braglia, R. Stocker, T. Amietszajew, A. J. Roberts, R. Bhagat, D. Billsson, J. Z. Olson, J. Park, G. Hinds, A. Ahlberg Tidblad, D. J. L. Brett, P. R. Shearing, *J. Electrochim. Soc.* **2020**, *167*, 120530.

Manuscript received: May 30, 2022

Revised manuscript received: August 8, 2022

Accepted manuscript online: August 15, 2022

Version of record online: September 7, 2022